Université de Montréal

H3$^{K27M/I}$ mutations promote context-dependent transformation in acute myeloid leukemia with *RUNX1* alterations

par Yu Wei Zhang

Programme de Biologie Moléculaire
Faculté de Médicine

Thèse présentée
en vue de l'obtention du grade de Maitrise
en Biologie Moléculaire
option Générale

August 2017

Résumé

Les mutations néomorphiques faux-sens affectant certaines lysines critiques des histones H3 jouaient un rôle important dans le développement d'une grande variété de tumeurs solides. Malgré la forte prévalence des mutations $H3^{K27M}$ dans les glioblastomes pédiatriques, se traduisant par une perte globale de H3K27me2/3, ces mutations n'ont pas été étudiées dans les cancers hématologiques humains. En utilisant les transgènes $H3.3^{K27M/I}$, nous avons étudié les effets d'une perte de H3K27me2/3 sur les cellules hématopoïétiques normales et transformées.

Nous avons identifié des mutations d'histone $H3^{K27M/I}$ dans des leucémies myéloïdes aigües (LMA) accompagnées d'une diminution significative de H3K27me2/3. Les profils mutationnels des patients H3K27M/I a révélé que ces lésions génétiques survenaient invariablement de manière concomitante avec des mutations affectant le gène RUNX1. L'expression ectopique de $H3^{K27M/I}$ dans un modèle murin de leucémie induite par AML-ETO9a a accéléré la prolifération cellulaire in vitro et le développement leucémique in vivo. Cependant l'expression de $H3.3^{K27M}$ dans des cellules hématopoïétiques humaines CD34+ de sang de cordon a mené à une expansion sélective d'une population primitive de progéniteurs mais n'a pas été suffisante pour induire seule le développement leucémique.

Ces résultats démontrent l'existence d'une collaboration entre RUNX1 et la perte de H3K27me2/3. Dans un contexte de LMA avec mutation RUNX1, l'hypo-H3K27me3 accélère la progression de la maladie. Nous concluons que H3K27me2/3 possède une activité suppressive des LMA mutées dans RUNX1. Nos résultats ont le potentiel de guider le développement d'une approche thérapeutique ciblée pour le traitement des LMA avec mutations RUNX1.

Mots-clés: les cellules hématopoïétiques, leucémies myéloïdes aigües, $H3.3^{K27M/I}$, oncohistones, RUNX1, Leucegene

Abstract

Neomorphic missense mutations affecting crucial lysine residues in histone H3 genes have been shown to be initiating mutation in a variety of solid tumors. Despite the high prevalence of *H3*^{K27M} mutations in pediatric glioblastoma proceeded by the loss of global H3K27me2/3, these mutations have not been studied in human hematological cancers. Using the *H3.3*$^{K27M/I}$ transgenes we studied the effects of the loss of H3K27me2/3 on normal and transformed hematopoietic cells.

We identified oncogenic histone *H3*$^{K27M/I}$ mutations in human acute myeloid leukemia (AML) that led to a significant reduction of H3K27me2/3. The mutation profiles of H3$^{K27M/I}$ patients revealed that these lesions invariably co-occurred with *RUNX1* alterations. Expression of H3.3$^{K27M/I}$ in an *AML1-ETO9a* driven mouse model resulted in accelerated *in vitro* proliferation and *in vivo* disease latency. The expression of H3.3^{K27M} in human CD34^{+} umbilical cord blood cells led to a selective expansion of a primitive hematopoietic progenitor population, but was insufficient to drive leukemogenesis on its own.

This demonstrates a collaboration between RUNX1 and loss of H3K27me2/3. In the context of RUNX1 alterations in AML, hypo-H3K27me3 accelerates disease progression. We conclude that H3K27me2/3 has a leukemia suppressive function in RUNX1 mutant and translocated AML. Our findings have the potential to inform the development of a targeted therapeutic strategy for the treatment of RUNX1^{mut} AML patients.

Keywords: Hematopoietic Stem Cells. Acute Myeloid Leukemia, H3.3 $^{K27M/I}$, oncohistones, RUNX1, Leucegene

Table des matières

Liste des figures

Chapter 1

Chapter 2

Liste des tableaux

Liste des sigles

Acute lymphocytic leukemia (ALL)
Acute myeloid leukemia (AML)

Bone marrow (BM)

ChIP-sequencing (ChIP-seq)
Chronic myeloid leukemia (CML)
Clustered regularly interspaced short palindromic repeats (CRISPR)
Core-binding factor (CBF)
Colony forming unit (CFU)
Common myeloid progenitor (CMP)
Common lymphoid progenitor (CLP)

Diffuse intrinsic pontine glioma (DIPG)
Diffuse large B-cell lymphoma (DLBCL)
DNA methyltransferase (DNMT)

Embryonic ectoderm development (EED)
Embryonic stem cell (ESC)
Encyclopedia of DNA Elements (ENCODE)
Enhancer of Zeste 1 (EZH1)
Enhancer of Zeste 2 (EZH2)

Glioblastoma multiforme (GBM)
Granulo/erythroid/monocytic/megakaryocytic (GEMM)
Granulocyte-macrophage progenitor (GMP)

Hematopoietic stem cell (HSC)
Hematopoietic stem and progenitor cell (HSPC)

Histone deacetylase (HDAC)
Histone demethylase (HDM)
Histone methyltransferase (HMT)

Leukemia stem cell (LSC)
Limiting dilution assay (LDA)
Long-term hematopoietic stem cell (LT-HSC)
Lysine-to-methionine (KM)

Mix lineage leukemia (MLL)
Multiplicity-of-infection (MOI)
Multipotent progenitors (MPP)
Myelodysplastic syndrome (MDS)
Myeloproliferative neoplasm (MPN)

Polycomb repressive complex 1 (PRC1)
Polycomb repressive complex 2 (PRC2)
Post-translational modification (PMT)

RNA interference (RNAi)
Runt-related transcription factor (RUNX)

S-adenosyl-methionine (SAM)
Short-term hematopoietic stem cell (ST-HSC)
Suppressor of zeste 12 (SUZ12)

The Cancer Genome Atlas (TGCA)
Transcriptional factor (TF)

Umbilical cord blood (UCB)

Variant allele frequency (VAF)

Liste des abréviations

For example (e.g.)

That is (i.e.)

Remerciements

In writing this memoire, I have had the opportunity to reflect on the last two years of my Master's and realized that I have been extremely fortunate to be surrounded by so many talented and generous people who made this work possible. The experiences and knowledge that I will take from IRIC will continue to shape my PhD and for years beyond that.

First and foremost, I would like to thank my research director, Dr. Guy Sauvageau for the opportunity to join his team. It is rare to find a supervisor that has exceed in so many areas of science. The incredible experiences that I have had at IRIC would not have been possible without the members of the team that he has assembled.

A special thanks to Bernhard Lehnertz for being a patient and thoughtful supervisor. I am extremely fortunate to have a found a mentor that who has allowed me to grow scientifically. Thank you to Tara MacRae, Jalila Chagraoui, Elisa Tomellini, Richard Bisaillon, Irene Baccelli and Laura Simon for your guidance and the many hours of discussions. Finally, to Julie Lessard and Alain Verreault, for being a part of my Master's committee.

In closing, I believe the years that I have spent in the Sauvageau Lab was a period of remarkable growth for me as a scientist. This was thanks to the collaborative effort of everyone at the IRIC to provide opportunities for young scientists and build a collaborative research environment. Finally, this work would not have been possible without a community that values science and the generous support of FRQS.

CHAPTER 1 – INTRODUCTION

Chromatin Biology

The primary function of the chromatin is to efficiently package the mass quantity of DNA to fit into the nucleus. The chromatin consists of complexes of small proteins known as histones that are wrapped around by DNA. The tight or loose wrapping of the DNA around the histone regulates DNA replication, DNA damage, recombination, transcription and most importantly controls whether the genes can be expressed to form their encoded product. Chromatin packaging is highly dynamic and is governed by different chromatin modifying activities such as DNA methylation, histone modification, and ATP-dependent remodeling. The term "epigenetic" was coined to describe these changes that modified gene expression without alterations in DNA sequence.

1.1.1 Chromatin Structure

At its most fundamental level, chromatin structure is comprised of the nucleosome, a structure containing an octamer of four core histone proteins which is wrapped around by 147 base pairs (bps) in 1.7 turns around a protein octamer. The nucleosome core particle is composed of a hetero-octamer of histones comprising a tetramer of $(H3\text{-}H4)_2$ flanked by two dimers of H2A-H2B. Each histone is composed of a globular domain and an unstructured tail domain. Two consecutive nucleosomes can be bound by linker histone H1. Together, the repeating structure of nucleosomes result in the formation of a structure that resembles "beads on a string" **(Figure 1)**. Nucleosomes coil and stack together forming chromatin, which is condensed into higher-order structures and compacted into the chromosomes [1, 2]. Components of chromatin such as the histone protein and DNA are chemically or structurally modified to decrease or increase accessibility to regulatory proteins. For instance, a tight compaction restricts the regulatory elements of the gene to be inaccessible to the regulatory proteins, thereby blocking gene expression [3].

Multiple histone variants exist for the core histone H3, H2A, H2B and for the linker histone H1. Often, the histone variants only differ by a few amino acids or domains. Each variant localizes to specific chromatin domains and may be differentially expressed in various tissues. The substitution of the core histones with different variants will affect post-translational modifications (PMTs), protein interaction and higher order chromatin structure [4].

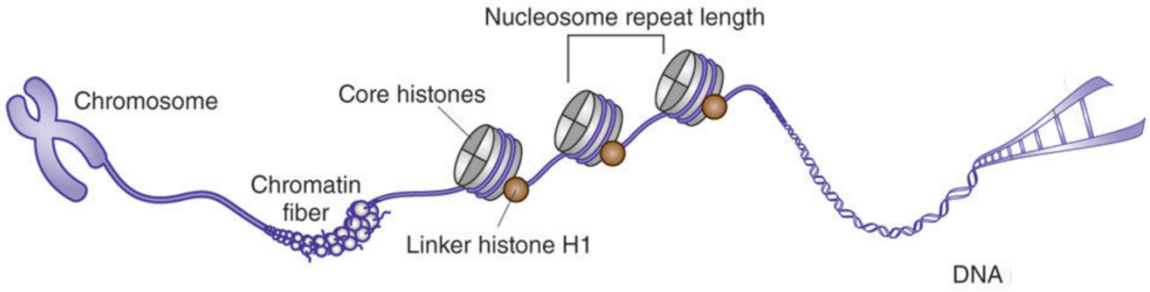

Figure 1. Illustration of Chromatin Compaction. Double helix DNA wraps around a histone octamer that contains two copies of the major types of histones (H2A, H2B, H3 and H4) and connect through the linker histone H1 to form the nucleosomes. The nucleosomes further condense into chromatin fibers to be package into the nucleus. Modified from [5].

Chromatin is traditionally distinguished in two forms: euchromatin and heterochromatin. These terms were coined by Emil Heitz, who had observed heterochromatin as chromosomal segments that appeared extremely condensed and dark in the nucleus during interphase. In contrast, euchromatin appeared relatively light in color [6]. Since then, we have uncovered that euchromatin is less condensed and can be transcribed, whereas heterochromatin is highly condensed and cannot be transcribed. Heterochromatin can be further categorized into facultative and constitutive heterochromatin. Constitutive heterochromatin occupies the same regions (centromeric and telomeric chromosome) in every cell and in regions that are gene-poor. In contrast, facultative heterochromatin is associated with the silencing of genes due to developmental/environmental cues and scatters throughout the genome. These differing chromatin regions within the genome are marked by a variety of PTMs that give the regions their identity [7, 8].

1.1.2 Chromatin Regulation by Histone Post-Translational Modifications

The observation that histone modifications regulate specific and distinct functional outputs of the eukaryotic genome has led to the histone code hypothesis. Due to the structural protruding of the histone tail, the amino acids on the tail are easily accessible targets to enzymatic activities that form PTMs. Histone modifications occur on serine, lysine and arginine residues of the N-terminal tail of the four core histones. These residues can undergo methylation, acetylation, phosphorylation, ubiquitination or sumoylation **(Figure 2)** [9]. The post-translational enzymes are referred as "erasers" and "writers" referring to their ability to deposit or remove PTMs from the histone. PTMs are dynamically regulated, with many enzymes dedicated to their addition and removal. The numerous post-translational modifiers each target specific residues and can deposit/remove a specific modification. The interpretation of the modification depends on the "reader/effector" that will bind to a specific combination of histone modification and translate the code into a meaningful biological consequence [3, 10].

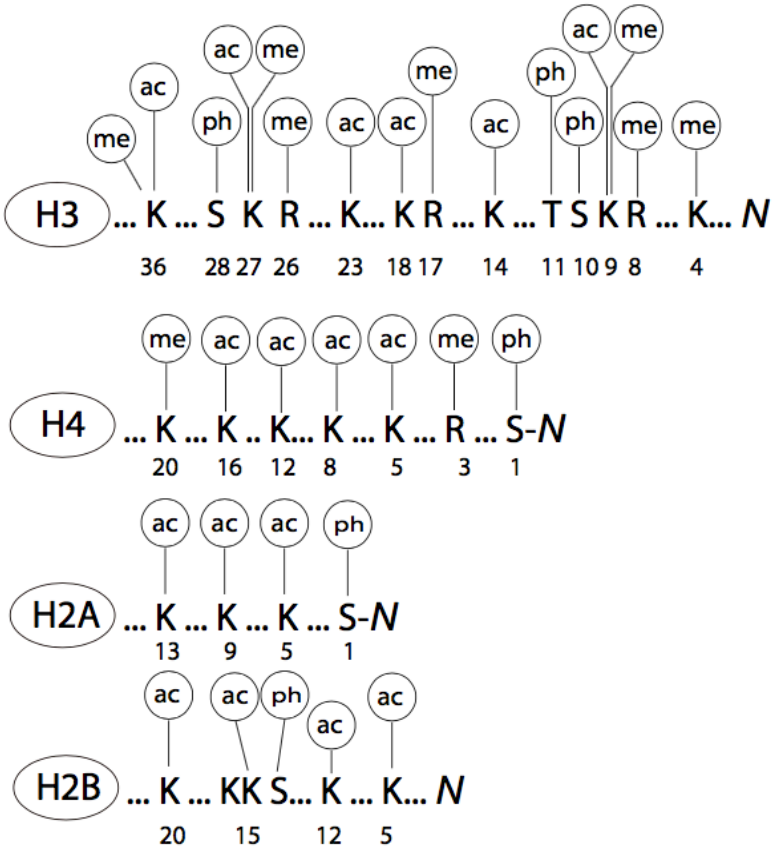

Figure 2. Illustration of Histone Modifications. The N terminal tail of the histones protrude from the core of the nucleosome and are subject to a variety of modifications that influence chromatin structure. PTMs establish a signaling platform to recruit reader modules. The readers determine the functional outcome of the PTMs. The different post-translational modifications that can occur on each histone are illustrated in this figure. Adapted from [11].

Genome wide pattern analyses of PTMs at regulatory regions (i.e. promoter and enhancer) have shown that PTMs associate at functionally distinct genomic regions and are successfully used to predict the presence of regulatory elements. For instance, H3K9ac and H3K4me2 tend to correlate with active promoters and H3K4me1 is present at distal enhancer regions **(Table 1)** [12].

Histone modification	Signal Characteristics	Association in the Genome
H3K4me1	Peak/region	Associated with enhancers, distal elements, and enriched downstream of transcription start sites
H3K4me2	Peak	Associated with promoters and enhancers
H3K4me3	Peak	Elements primarily associated with promoters/transcription starts
H3K9ac	Peak	Associated with promoter regions
H3K9me1	Region	Preference for the 5′ end of genes
H3K27ac	Peak	Mark of active regulatory elements; may distinguish active enhancers and promoters from their inactive counterparts
H3K27me3	Region	Repressive mark established by polycomb complex activity
H3K36me3	Region	Elongation mark associated with transcribed portions of genes
H3K79me2	Region	Transcription-associated mark, with preference for 5′ end of genes
H4K20me1	Region	Preference for 5′ end of genes

Table 1. Overview of histone modifications and their associated genomic region. The systemic mapping of transcription and transcription factors association through the Encyclopedia of DNA Elements (ENCODE) project identify that different histone modifications can be used systematically to assign functional attributes to genomic regions. Table modified from [12].

1.1.3 Histone Modification: Methylation

Lysine methylation has a diverse number of roles that include heterochromatin formation, X-chromosome inactivation, and transcriptional regulation. Unlike acetylation which generally

correlates with transcriptional activation, histone lysine methylation can signal either activation or repression depending on the site of methylation [13]. The lysine methylation sites that have been associated with transcriptional activation include K4, K36 and K79 on histone H3. In contrast, di- and trimethylation of K9 and K27 on histone H3 are associated with transcriptional repression [14]. The degree of histone lysine methylation is determined by the antagonizing activities of site-specific histone methyltransferases (HMTs) and histone demethylases (HDMs). Almost all histone lysine methyltransferases rely on the catalytic activity of the SET domain for the addition of methyl-groups on the lysine residue [15] (DOT1/DOT1L is the only lysine methyltransferase that lacks a SET domain [16]). The two most conserved motifs within the SET domain (i) is a tyrosine which is essential for interacting with the lysine, and (ii) a knot like structure that is the S-adenosyl-methionine (SAM) binding pocket. The co-factor SAM serves as the methyl group donor for the covalent modification [17]. The removal of the methyl mark is achieved through the catalytic activity of histone lysine demethylases, amino oxidase or the JMJC family[18, 19].

At the core of the H3K27 silencing system is Polycomb Repressive Complex 2 (PRC2) which is composed of either methyltransferase, Enhancer of Zeste 2 (EZH2) or its paralog Enhancer of Zeste 1 (EZH1). EZH2 functions with the assembly of other PRC2 proteins at the N terminal domain that include Embryonic Ectoderm Development (EED) and Suppressor of Zeste 12 (SUZ12). The catalytic SET domain of EZH1/2 deposits the repressive H3K27me2/3 mark which inhibits the accessibility of transcription factors through chromatin compaction. In addition, accessory subunits that influence PRC2 activity can be present in the complex including histone-binding protein RBBP4, zinc finger protein AEBP2 and PHF1 **(Figure 3).** Multiple factors influence recruitment of PRC2 to its genomic target including the DNA sequence, transcription factors and pre-existing histone modifications. [20, 21].

Specific histone demethylases are involved in the removal of histone methylation marks. The lysine 27 methyl marks catalyzed by EZH1/2 are removed by the demethylase activity of HDMs, UTX and JMJD3. JMJD3/UTX are part of the KDM6 subfamily that contains a well-conserved JMJC domain in their C terminus which catalyzes the transition of H3K27me3 to H3K27me2 to H3K27me1, transitioning from a repressive to an active chromatin conformation

[22]. In summary, it is the dynamics between HDM and HMT activity that modulates gene expression.

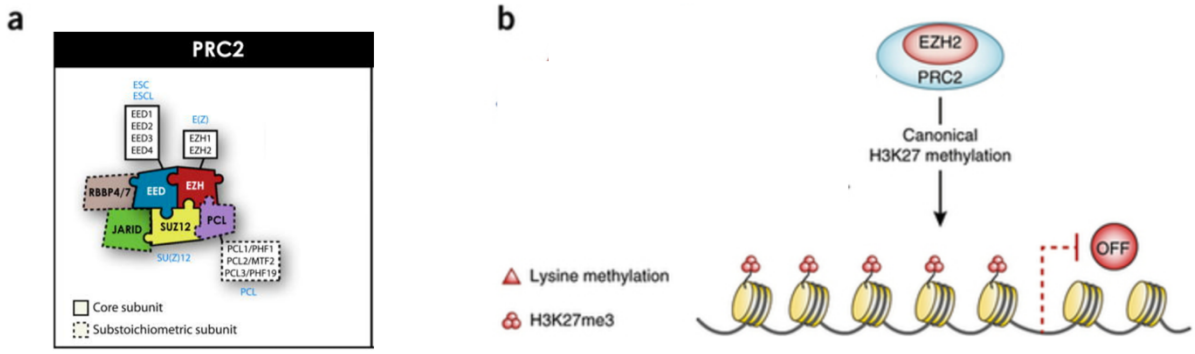

Figure 3. The Polycomb Repressive Complex 2 in coordinating epigenetic silencing activity. (a) The mammalian PRC2 is composed of three essential core subunits: the catalytic subunit Enhancer of Zeste 2 (EZH2) or Enhancer of Zeste 1 (EZH1), Embryonic Ectoderm Development (EED) and Suppressor of Zeste 12 (SUZ12). The accessory proteins of the PRC2 include PCL, RBBP4/7 and JARID that modulate PRC2 activity in different cellular contexts. (b) EZH2 mainly regulates transcriptional activity through the methylation of H3 on lysine 27 (H3K27) that is associated with gene silencing. Adapted from [21] and [23].

Stem Cell Biology

Throughout the life time of an individual, hematopoietic stem cells (HSCs) are responsible for replenishing the blood and immune cells. HSC differentiation is achieved through stepwise restriction of lineage potential. HSCs remain quiescent for most of their lifespan, while the more committed progenitors have very high proliferative capacities. For instance, HSCs give rise to a series of multipotent progenitors (MPPs) that have decreased self-renewal potential. MPPs differentiate towards more committed progenitors and eventually produce the mature cells that constitute the blood and the immune system **(Figure 4)**. The balance between self-renewal, differentiation and proliferation in the hematopoietic lineage is critical for maintaining homeostasis and enables the rapid and robust response to physiological stresses, such as blood loss, infections and traumatic injuries [24].

It remains to be elucidated exactly how a stem cell determines whether to maintain its multi-potency or to differentiate. However, we can speculate that this process involves a fine

orchestration between cell cycle regulation and cell fate decision. During the transition from HSC to committed progenitor, there is a down-regulation of many HSC-associated genes which inversely correlate with the up-regulation of lineage-specific genes. The silencing or activation of gene expression and transcriptional programs is controlled by a highly regulated epigenetic process of DNA methylation and histone PTMs [24].

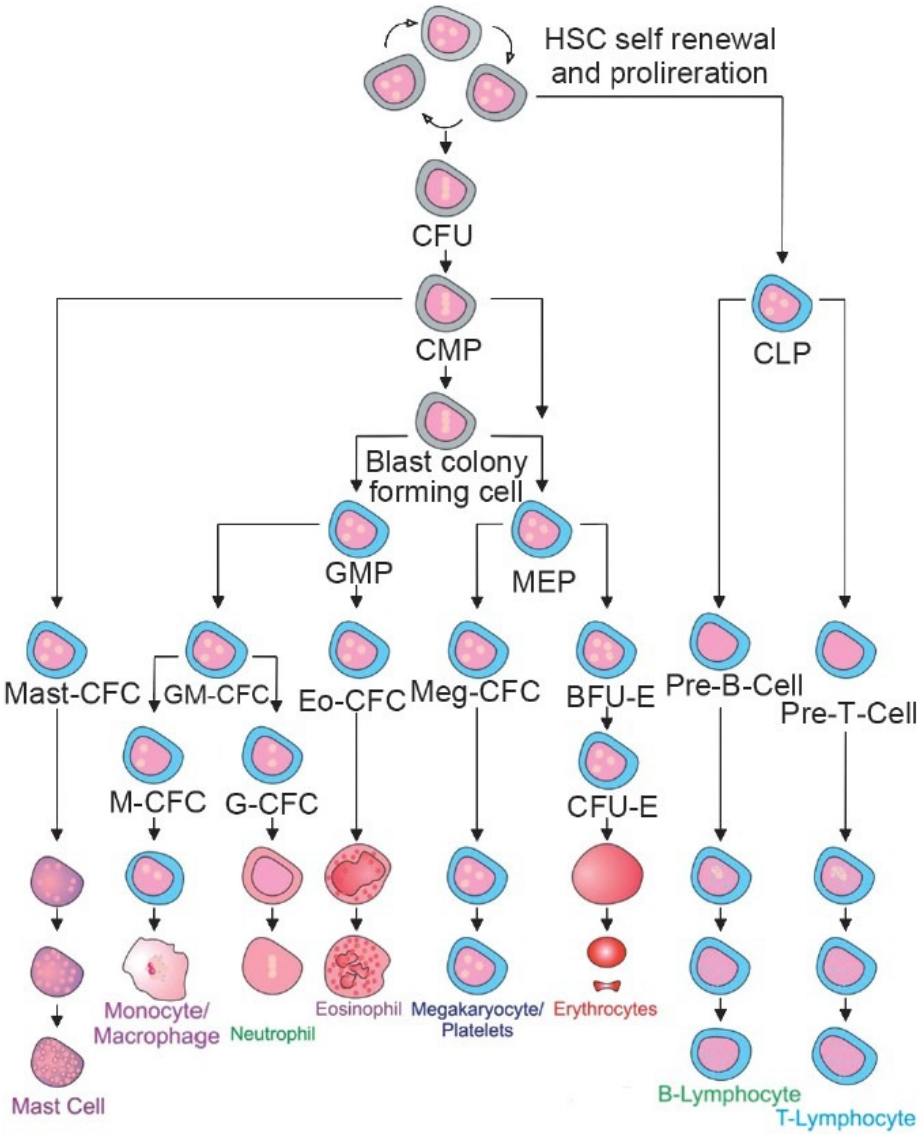

Figure 4. Hematopoietic stem cell hierarchy. Hematopoietic stem cells give rise to several multipotent progenitors — colony-forming units (CFUs) that differentiate into common myeloid progenitor (CMP) and common lymphoid progenitors (CLP) which in turn produce

oligopotent progenitors (i.e. granulocyte-macrophage progenitors (GMP) and megakaryocyte/ erythrocyte progenitors (MEP)) and eventually fully differentiated cells (i.e.monocyte/macrophages/granulocytes and megakaryocytes/ platelets/ erythrocytes) [25].

1.1.4 Epigenetic Regulation of Normal Hematopoiesis

All cells of the hematopoietic lineage share the same genome but differ in their epigenome. During cellular division, dynamic changes occur in the epigenetic landscape allowing them to acquire their cellular identity.

A phenomenon that was originally demonstrated in embryonic stem cells (ESCs) describing key developmental genes that were simultaneously occupied by counteracting marks has also been reported in HSCs. These bivalent domains constitute the co-existence of repressive H3K27me3 and activating H3K4me3 marks. This mechanism ensures silencing while enabling quick activation [26]. Genome wide association mapping has identified an association of developmental genes with bivalent chromatin marks in HSCs and MPP cells. During lineage commitment, the bivalent marks will dissolve taking on the identity of being either repressive or activating. Interestingly, regions that become activating after lineage commitment associated with H3K4me1 and H3K27me1 in the gene regulatory regions. Overall this would suggest, the commitment to a specific mark during differentiation is already predetermined in HSCs and MPP cells [27].

PRC2 plays a major role in normal hematopoiesis by promoting pluripotency maintenance and self-renewal of hematopoietic stem cells. Interestingly, PRC2 regulates normal hematopoietic stem cell function in a developmental-stage-specific manner. For instance, the deletion of Eed exhausts adult HSCs, whereas neonatal HSCs are produced in normal numbers but are defective in maintenance/differentiation [28]. Furthermore, loss-of-function mutation of Ezh2 or Suz12 enhanced the activity of HSC and progenitor cells. By silencing pro-differentiation genes in LT-HSCs, Ezh2 maintains long-term self-renewal potential. The ectopic expression of Ezh2 causes a significant increase in HSCs and myeloid lineage cells [29]. In addition, the over-expression of Ezh2 in HSCs prevents exhaustion and maintains stem cell

potential over a series of transplantations [30]. This was in line with the observation that Ezh2 is abundantly expressed in highly purified HSCs and is rapidly down-regulated on differentiation. The ability of PRC2 to maintain HSCs may rely on its repression of Cdkn2a. Normally, Cdkn2a induces cycle arrest in G1 and G2 but is repressed by H3K27me3. The deletion of Cdkn2a partially rescues HSC deficiency in Eed($^{-/-}$) mice. Ezh2 also represses genes associated with cell cycling, HSC differentiation and pro-apoptosis (e.g. *NOXA*, *p21* and *WIG1)* [28, 31]

During lymphopoiesis, Ezh2 expression is up regulated in proliferating cells such as human germinal center B cells, cycling T and B lymphocytes and plasmablasts. Then during B-cell differentiation and maturation, Ezh2 becomes down-regulated. This suggests that EZH2 acts as a checkpoint mechanism that regulates pro-B to pre-B cell transition. In support of this EZH2 was shown to regulate pre-B cell receptor in pro-B cell, a receptor implicated in both cycle exit and Igκ recombination expression [32]. In addition, Ezh2 can also inhibit the maturation of pro- to pre- B cells through Stat5 mediated recruitment of Ezh2 to repress Igκ transcription thereby inhibiting recombination [33].

1.1.5 Hematopoietic Malignancies

In many respects, leukemia cells share many common characteristics of a normal hematopoietic stem cell. Pathways classically associated with cancer also regulate normal stem cell function such as proliferation, survival, self-renewal and differentiation. Mutations can occur at any point during stem cell division and give rise to a leukemia-initiating mutation. Evidence suggests that the first leukemogenic mutations occur in a self-renewing cell (i.e. HSC) or in a more differentiated cell (i.e. MPP) to re-establish the ability to self-renew. These initial mutations confer pre-leukemic cells that will go on to accumulate successive mutations, and lead to the loss of normal hematopoietic functions and subsequently the formation of blast cells. In many cases, only one or two additional cooperating mutations are needed to generate the malignant founding clones [34, 35].

1.1.6 Acute Myeloid Leukemia

Acute myeloid leukemia (AML) is characterized by a block in myeloid differentiation and the uncontrolled proliferation of transformed myeloid progenitors. Current paradigms suggest that AML can be a (1) a step-wise progressive malignancy. When myelodysplastic syndromes (MDS) or myeloproliferative neoplasms (MPN) are untreated, they can progress into chronic myeloid leukemia (CML) and ultimately evolve to become AML. Alternatively, AML can develop from (2) genotoxic therapies from unrelated malignancies, but most cases arise (3) *de novo*. The increased effort to characterize mutations occurring in AML have revealed key insights into mechanisms of leukemogenesis [36].

AML is a rapidly progressing disease, and treatment needs to commence almost immediately after diagnosis. Treatment for AML usually consists of high dose chemotherapy and/or stem cell transplantation. Chemotherapy is highly successful at inducing remission of AML patients, but there is a high probability of relapse [37]. Newly developed technologies in next generation sequencing (NGS)/RNA sequencing (RNA-seq) have revealed large molecular heterogeneity of the disease and allowed for better characterization. These advancements have driven the development of precision medicine that is directed at targeting specific mutations. The translation of these advancements into improved therapy is just beginning. Overall, AML is a clinically and genetically heterogeneous disease that is marked by a multitude of chromosomal abnormalities and/or genetic alterations which translate to differences in drug response and survival.

There is a close connection between stem cell differentiation and wide-spread epigenetic remodeling. Epigenetic alterations are observed in several hematological malignancies, consistent with data from clinical patients describing epigenetic regulator mutations. The Cancer Genome Atlas(TCGA) performed whole exon sequencing of 200 AML patients, and revealed that 30% of mutations are within chromatin modifiers (e.g. ASXL, EZH2, MLL-PTD), 44% in DNA modification genes (e.g. DNMT3A, TET2, and IDH1/2) and myeloid transcription factors (e.g. CEBPA, RUNX1) [38]. The prevalence of mutations in epigenetic modifiers make them an attractive drug target for treatment.

1.1.7 EZH2 in Disease Hematopoiesis

Genetic and epigenetic profiles can influence disease progression thereby understanding these aberrations can provide insight into the mechanism of tumorigenesis. The first indication of EZH2 being a driver mutation came from the observation that EZH2 over-expression was associated with poor prognosis in prostate cancer patients [39]. Since then, high EZH2 expression in tumour cells has been documented in breast, bladder and endometrial cancer correlating with aggressive and advanced disease stages [40].

The PRC group of chromatin regulators are critical for HSC lineage specification, but often become deregulated during leukemogenesis. For instance, somatic heterozygous point mutation at tyrosine 641 (Y641) in the SET domain of EZH2 increases global H3K27me3 and is found in 22% of diffuse large B-cell lymphomas (DLBCL) and in 7% to 12% of follicular lymphomas [41]. In line with this, *Yap et al*. (2011) proposed that the inactivation of UTX results in increased H3K27me3 leading to the formation of blast cells, overall suggesting that hyper-H3K27me3 is an oncogenic mark [41]. These genetic studies have led to an intense effort to develop EZH2 inhibitors, that prevent methylation through inhibiting the SAM-binding pocket in the SET-domain of EZH2(e.g. GSK126 and UNC1999. Currently, there are eight EZH2 inhibitors and their therapeutic status varies between preclinical and phase I clinical trial [42, 43] **(Table 2).** Preclinical trials for GSK126 was performed in DLBCL and has progressed onto phase I clinical trial [42]. Similarly, UNC1999 which has been hailed as the inhibitor for both EZH1 and EZH2, has been shown to selectively kills DLBCL cells [44].

Although, gain-of-function mutation of *EZH2* in hematopoietic malignancies would suggest its role as a proto-oncogene, *EZH2* has also been characterized to be a tumour suppressor. Inactivating mutation of *EZH2* are often observed in T-ALLs, MDS and MPN [45, 46]. Overexpression of JMJD3 was found in cases of Hodgkin's lymphoma and is associated with the loss of H3K27me3 at derepressed target genes [47]. It clearly has been demonstrated the fluctuation of H3K27 methylation due to *EZH2* mutations has multi-faceted functions in hematological disorders that is highly context-dependent.

Compound	Mechanism	Status	Selectively On
DZNep	SAH hydrolase inhibitor of methyltransferase	Preclinical	Breast cancer cell lines(MCF7, MDA-MB-231 and SKBr3), mesothelioma see lines (H28, H2052, and H2452), glioblastoma multiforme (CSC cultures from human GBM samples)
El1	SAM competitive inhibitor of PRC2	Preclinical	Diffused large B-cell lymphomas cells (EZH Tyr641 mutations)
EPZ005687	SAM competitive inhibitor of PRC2	Preclinical	Diffused large B-cell lymphomas(EZH2 Tyr641 or Ala677 mutation)
GSK343	SAM competitive inhibitor of PRC2	Preclinical	Prostate and Breast Cancer Cell Lines
GSK126	SAM competitive inhibitor of PRC2	Phase I	Diffused large B-cell lymphomas cells validation in xenograft mice
UNC1999	SAM competitive inhibitor of PRC2	Preclinical	Diffused large B-cell lymphomas cells (EZH2 Tyr641 mutation)
EPZ-6438	SAM competitive inhibitor of PRC2	Phase 1/2	human lymphoma cell lines bearing EZH2 catalytic domain point mutations with validation in xenograft mice

Table 2. EZH2 inhibitors and their status in clinical development. Modified from [23].

1.1.8 Inhibition of PRC2 Activity through H3K27 Mutation

Recently, lysine-to-methionine (KM) mutations affecting H3K27 have been reported in pediatric brain cancers, more specifically diffuse intrinsic pontine gliomas (DIPGs) and supratentorial glioblastoma multiforme (GBMs). Often, in glioma a missense mutation AGG encoding a lysine is mutated into ATG, and shifts the amino acid codon to a methionine on lysine 27 of histone H3. The identified missense mutations were found predominantly in the genes encoding H3.3, H3F3A and H3F3B, and to a lesser extent in the genes encoding H3.1, HIST1H3B and HIST1H3C. Non-canonical histone H3.3 is a replication independent histone, while canonical H3.1 and H3.2 are expressed for replication coupled deposition. These variants differ by four amino acids, but these residues have crucial roles in specialized functions and localization in the genome. For instance, terminal differentiate neurons are composed of 90% of H3.3 of total histone H3. Whereas in dividing cells, H3.3 comprises ~20% of total histone H3. Interestingly, the specific *H3.1* or *H3.3* mutations were found to differ by the tumour type, patient age and location. H3K27 mutations appear to be mutually exclusive with IDH1 mutation and EGFR amplification, and commonly associate with p54 overexpression and ATRX loss [48, 49].

$H3^{K27M}$ mutations were shown to have a potent dominant inhibitory effect on the EZH1/2 enzymes thereby causing a profound and specific reduction in H3K27me2/3 and a modest

increase in H3K27ac [50]. All other amino acid substitutions were surveyed for a reduction of methylation, at a lesser extend a histone lysine-to-isoleucine mutation(*H3^{K27I})* was also able to achieve reduced H3K27me3. Similarly, transgene over expression of lysine 4, 9, or 36 to methionine on H3*(to be referred as H3^{KM}*) subsequently resulted in the decrease of methylation on the corresponding lysine residue **(Figure 5)** [50]**.**

A histone lysine-to-methionine mutations targets the catalytic SET domain of HMTs, sequesters the enzyme and prevents binding with the endogenous H3. As little as 1% contribution from the mutated histone H3.3^{K27M} to total H3 was sufficient to cause a profound reduction in H3K27me2/3, with little changes to other histone marks. Reduction of histone methylation is achieved through a low expression level of the mutated histone due to the strong hydrophobic interaction occurring between the substituted methionine binding with the catalytic SET domain. Y641N mutation in the SET domain of EZH2 results in a less potent inhibition by H3^{K27M} peptide. This suggests that the aromatic-hydrophobic interaction plays a role in the stabilization of EZH2 at the lysine mark [50]. Recently, the crystal structure of EZH2 and an H3^{K27M} peptide revealed that the methionine residue rests in the pocket that normally accommodates the lysine residue in the SET domain. The H3.3^{K27M} substitution has a stronger binding of EZH2 due to the (1) unbranched hydrophobic residue that leads to stronger binding; (2) high avidity due to SUZ12 and RbAp48 binding to H3. Overall, K27M mutant nucleosomes have a 22-fold higher affinity to EZH1/2 compared to the wild type lysine residue, thereby sequestering the enzyme and efficiently inhibiting H3K27me3 [51].

GSK-J4 was developed as a specific inhibitor for UTX/JMJD3 through inhibition of the catalytic JMJC domain, and leads to an increase in H3K27me2/3 [52]. *In vitro* treatment of patient samples revealed a dose-dependent inhibition of cellular viability using GSK-J4 that was specific to H3.3^{K27M} mutated specimens [53]. Together, this provided evidence that histone alterations can directly promote tumorigenesis and that these tumors could be sensitive to K27 demethylase inhibition.

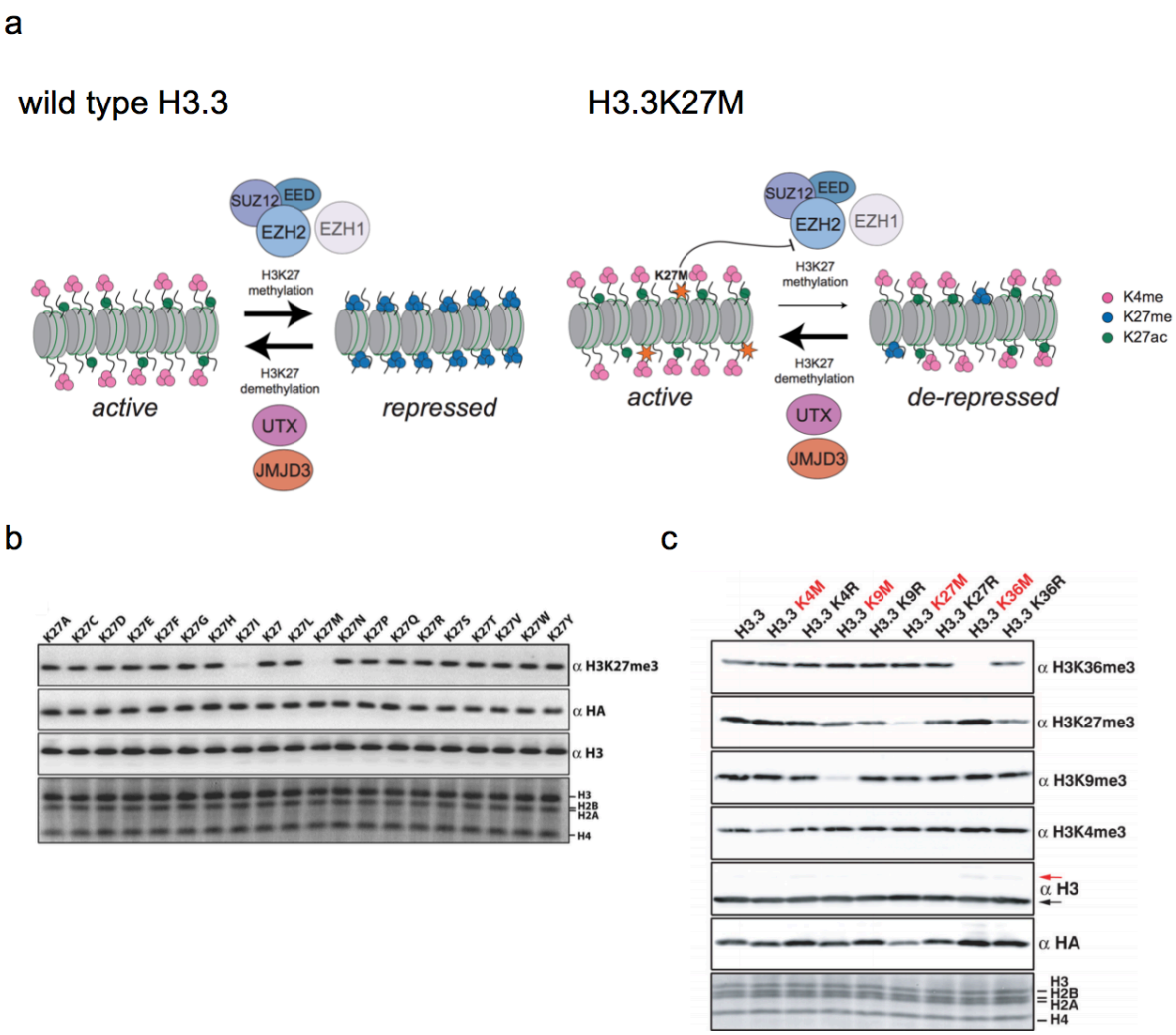

Figure 5. H3^{K27M} inhibits PRC2 methyltransferase activity. (a) K27M targets the catalytic sites of EZH1/2 competing with its endogenous substrate binding and inhibiting its ability to deposit H3K27me2/3. (b) A survey of all amino acid substitutions at H3K27 demonstrate that K27M reduces H3K27me3 and to a lesser extent K27I. (c) Other SET-domain proteins are sensitive to lysine-to-methionine substitution. H3.3 transgenes of K4M, K9M, and K36M decreased overall amounts of H3K9me2/3, H3K36me2/3 and a small reduction in H3K4me2/3. Modified from [50].

Gene Expression Regulation by Transcriptional Factors

Transcriptional factors(TFs) are also key cellular components that control gene expression, just like epigenetic factors their activity can affect cellular identity. TFs are commonly deregulated in numerous disease and are a major class of cancer cell dependencies.

1.1.9 Structure Characterization of RUNX

RUNX proteins are part of a family of metazoan transcription factors that are essential for development, with multiple roles ranging from proliferation, differentiation, apoptosis and lineage differentiation. Within a mammalian cell, there are three RUNX genes: RUNX1, RUNX2 and RUNX3 each with diverse functions that depend on cell context [54].

Structurally, RUNX proteins have a highly conserved DNA-binding domain termed the Runt domain and a divergent C terminus that has both an inhibitory and activation domain. At the DNA binding domain, RUNX1(formally known as AML1) interacts with its co-factor, core-binding factor β (CBFβ) to form the CBF complex and stabilizes the interaction between RUNX1 and the DNA motif 5′-PuACCPuCA-3′ [55]. The functional diversity of RUNX is based on the multiple protein interactions taking place at the C terminus. The interacting partners of RUNX are the basis of their ability to function as either a transcriptional repressor or activator. For instance, RUNX1 tends to be a weak transcriptional regulator by itself but achieves its full level of activity when interacting with other proteins. Many chromatin regulators are interacting partners that are found at the C terminus including Polycomb Repressive Complex 1 (PRC1) (i.e. Bim1), Histone Deacetylase (HDAC) (i.e. HDAC1,3), H3K4 methyltransferase Mixed Lineage Leukemia (MLL) and p300 Acetyltransferase [56, 57].

1.1.10 RUNX1 Alterations in Leukemia

Approximately 5-10% of AML cases carry the RUNX1 mutation and frequently co-occur with complex gene mutation involving epigenetic modifiers (AXSL1, IDH2, KDMT2A, EZH2) and components of the spliceosome complex (SRSF2, SF3B1)[58]. Interestingly, *EZH2* mutations are rare in AML but found in higher frequencies within RUNX1 mutant and RUNX1-RUNX1T1 AML **(Figure 6)** [59, 60]. In the context of MDS, the loss of Ezh2 promoted the transformation of mouse HSCs expressing RUNX1S291fs mutants [61]. The poor outcome of

patients suffering from *RUNX1*^{mut} AML highlights the need to better understand the genetics of this disease and to develop more specific and efficient therapeutic strategies [56].

Approximately 10–15% of AML cases carry the t(8;21)(q21;q22) translocation, which involves the *RUNX1* and *CBFβ* gene [62]. At the molecular level, the t(8;21) translocation results in the creation of the novel fusion protein AML1-ETO (RUNX1-RUNX1T1). Specifically, the full length AML1- ETO has 752 amino acids, comprising of the N terminal portion of the Runt domain of RUNX1 with the four nervy homology regions (NHR1-4) of ETO. AML1-ET09a(AE9a) is a truncated version of AML1-ETO generated by alternative splicing during transcription and comprises of 575 amino acids [63]. The NHR2 within ETO is an essential interacting surface for oligomerization, leading to a stable transcription complex and interaction with transcriptional regulators that will promote early myeloid self-renewal and interferes proper hematopoietic differentiation [64]. Like *RUNX1*^{mut} AML, we observed an enrichment of cooperating lesions occurring in epigenetic modifier [60]. AML1-ETO expression acts as a negative dominant of RUNX1 activity and is associated with good prognosis core binding factor subgroup.

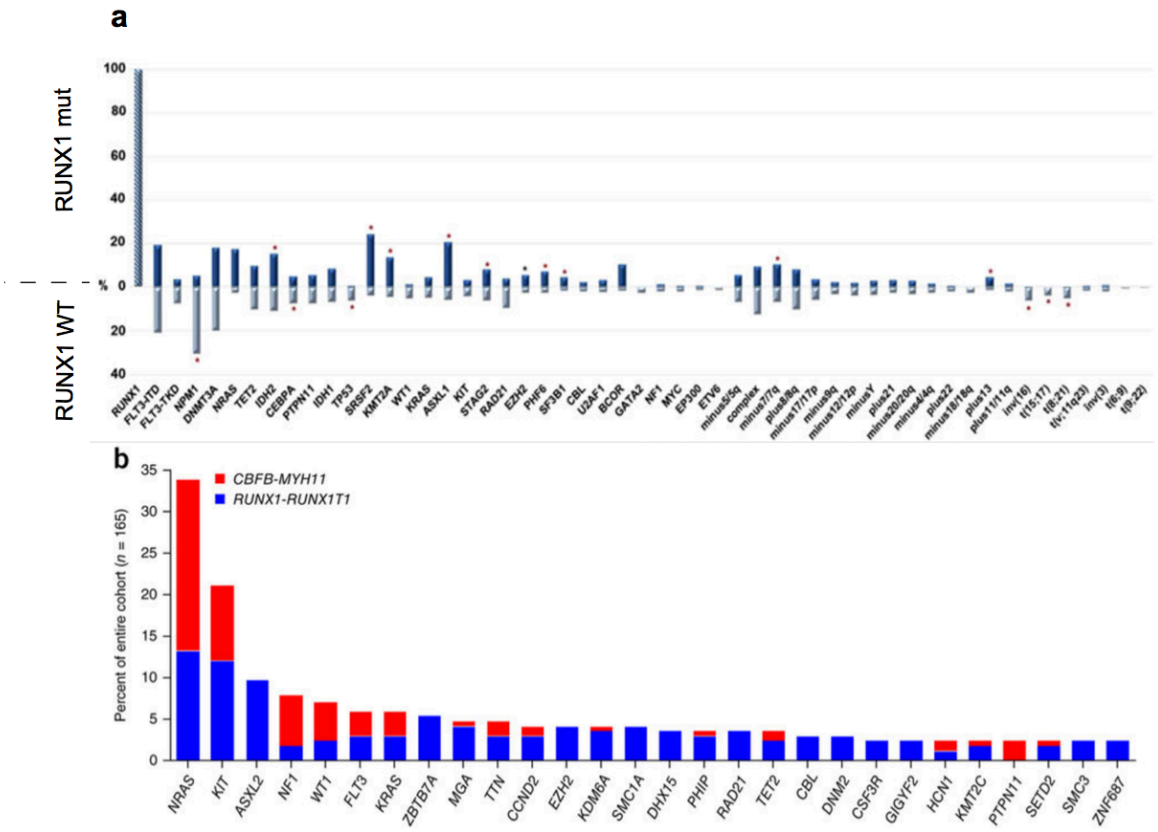

Figure 6. Organization of cooperating lesion in RUNX1^{mut} or t(8;21) AML. (a) Top axis represents mutation frequency of RUNX1^{mut} AML cooperating lesions. Bottom axis represents mutation frequency of RUNX1^{wt} AML cooperating lesions. The red/black asterisk marks represent significantly co-occurring cooperating lesions in either RUNX1^{mut} or RUNX1^{wt} AML. RUNX1^{mut} AML were significantly associated with mutations of epigenetic modifiers (ASXL1, IDH2, KMT2A, EZH2), components of the spliceosome complex (SRSF2, SF3B1) and STAG2, PHF6, BCOR (b) Mutation data for CBFβ–MYH11 and RUNX1-RUNX1T1 AML. Mutations in epigenetic modifiers (AXSL2, EZH2 and KDM6A) and cohesin (SCM1A, RAD21 and SMC3) were significantly enriched in RUNX1-RUNX1T1 AML represented in black bars. Both (a) and (b) showed that *EZH2* mutations predominately occur in the context of a RUNX1 alteration. Adapted from [60] and [59].

General Rationale and Hypothesis

In a series of landmark papers beginning in 2012, recurrent mutations in histone $H3^{K27M/I}$ were reported as frequently occurring mutations in adult/paediatric high-grade and diffuse intrinsic pontine glioma [48, 49]. Within the context of hematopoietic diseases, we observed $H3.3^{K27M}$ mutations in paediatric T-ALL, but presence of these histone mutations have not been reported in myeloid cancers to date [65]. However, inactivating mutations of EZH2 have been identified in MDS, MPN and AML [45, 46]. Furthermore, EZH2 mutations are rare in de novo AML, but a relative enrichment for PRC2 mutations have been observed predominantly in t(8;21) [57], RUNX1 mutant AML while they are virtually absent in inv(16) and RUNX1 wild type AML [58]. Based on this rationale, I can present the two hypotheses below.

Part I: I hypothesize histone H3K27 mutations may occur in AML.
Part II: If H3K27 mutations are present in AML, I hypothesize H3K27 mutations may occur in a specific genetic context.

My project will utilize Leucegene, one of the largest genomic and RNA sequenced collection of AML specimens consisting of 415 diseased patient samples. The tools provided through Leucegene will enable the scavenge for H3K27 mutations in AML specimens, but may also allow the identification of cooperating lesions, and quantification of H3K27me3 levels in the affected primary patient samples.

CHAPTER 2 – RESULTS

2.1 $H3^{K27M/I}$ mutations in Acute Myeloid Leukemia

2.1.1 Quantitative Analysis of H3K27me2/3 Through Flow Cytometry

To accurately quantify methylation, we needed to develop an easily applicable method to measure the level of H3K27me2/3 in *H3*.$3^{K27M/I}$ transgene expressing cells and in patient samples. Traditionally, western blot analyses have been used to measure H3K27me2/3. However, western blots have limited sensitivity and are unable to quantify methylation levels of individual cells. Flow cytometry provided a good alternative as it was widely used in clinical hematology and allowed us to examine heterogeneous cell populations at a single cell level in AML patient samples.

Development of this flow cytometry assay relied on the incidental discovery that OCI-AML5 had a significantly reduced level of H3K27me2/3 compared to OCI-AML3 **(Figure 7A)**. This dramatic reduction of H3K27me2/3 was explained by a homozygous point mutation (*R690H*) in the catalytic core of the EZH2 SET domain. The difference of H3K27me2/3 between OCI-AML5 and OCI-AML3 was then validated using flow cytometry and showed excellent agreement compared to the western blot thereby validating our protocol **(Figure 7B).** Using a 1:1 mixture of OCI-AML3 and OCI-AML5 cells, we efficiently titer our monoclonal H3K27me2/3 antibody, and determined the optimal dilution to be at 1/100 and the secondary antibody at 1/500 **(Figure 7C)**. Accurate measurement of H3K27me2/3 relied on normalization of the methylation signal to the total H3 content as H3K27me2/3 can increase dramatically in cases of hyperploid and variations in cycle cell. To normalize our H3K27me2/3 signal to the variation of nuclear DNA content, we titered an H3 antibody and determined the optimal dilution at 1/200, and the secondary antibodies at 1/500 **(Figure 7D)**. Using this dual antibody staining, we normalized H3K27me2/3 to H3 signal in FlowJo allowing us to reliably measure H3K27me2/3 in patient AML samples.

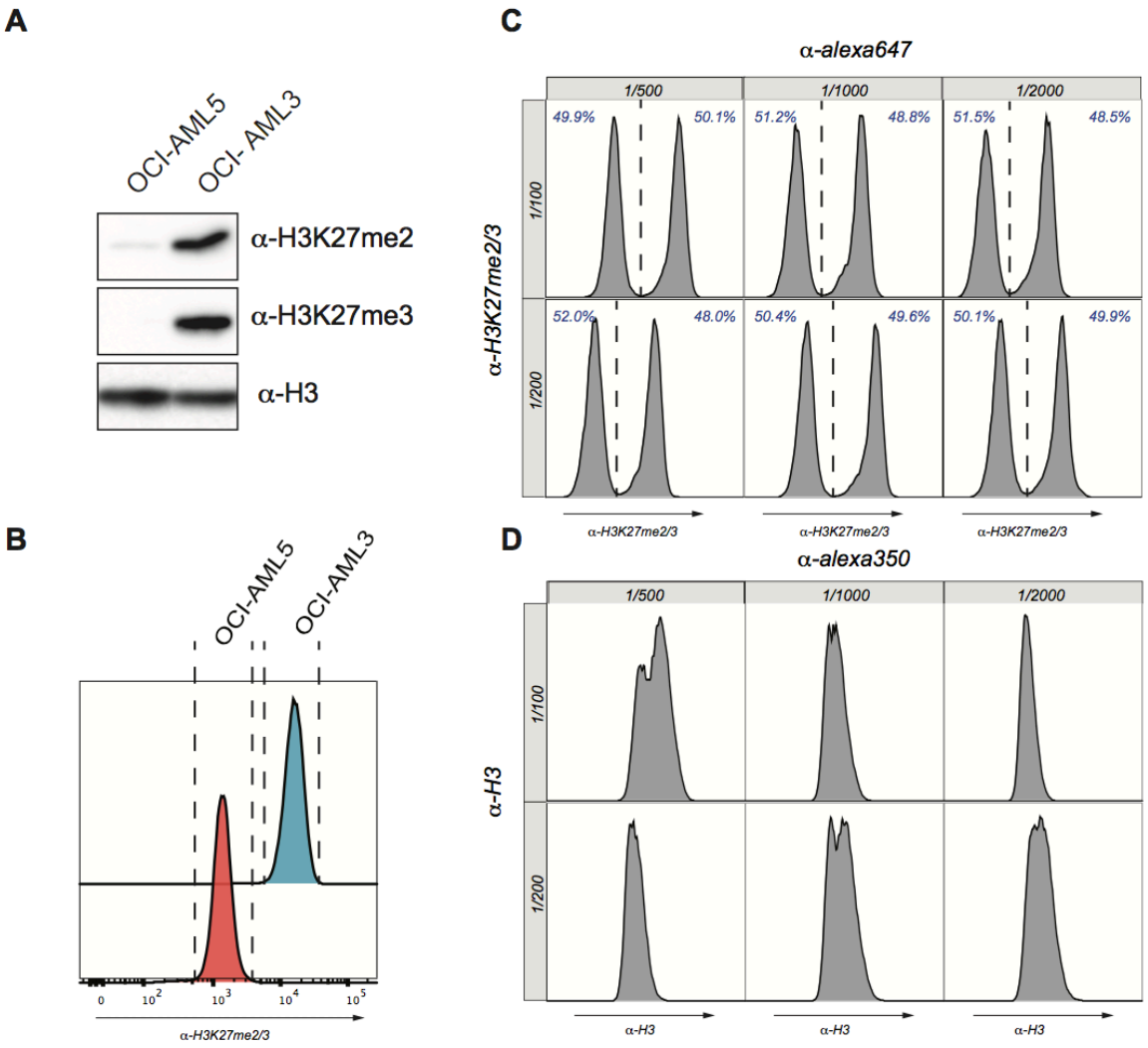

Figure 7. Establishment of a FACS-based assay to quantify global levels of H3K27me2/3

(A) Western blot analysis from whole cell lysates of OCI-AML 3 and OCI-AML 5. OCI-AML3 and OCI- AML5 have sharply contrasting levels of H3K27me2/3. (B) Flow cytometry on OCI-AML3 and OCI-AML5 cells reflected results from western blot analysis. OCI-AML3 had a significantly higher H3K27me2/3 signal in comparison to OCI-AML5. (C and D) Titration of H3K27me2/3 and H3 antibody. Histogram represents the H3K27me2/3 or H3 signal. Vertical axis shows different dilutions of primary antibody. Horizontal axis indicates the different dilutions of secondary antibody. Percentage of low and high H3K27me2/3 are represented in blue.

To validate the sensitivity of our flow cytometry assay, we cultured OCI-AML3 and OCI-AML5 cells in the presence of DMSO, UNC2400, UNC1999 or GSK126 for 72 hours. UNC1999 and GSK126 served as inhibitors of EZH1/2, while UNC2400 was the inactive molecule that was used as an additional control. Proceeding treatment, the cells were lysated for western blot analysis or fixed with ethanol for flow cytometry. Western blot analysis showed that OCI-AML3 treated with EZH inhibitors (UNC1999/GSK126) had significantly reduced H3K27me2/3 compared to the DMSO/UNC2400 controls. Similar, results were shown in the flow cytometry assay. By western blot, OCI-AML5 cells showed a complete loss of H3K27me2/3 regardless of the treatment condition. However, by flow cytometry OCI-AML5 treated with EZH inhibitors showed an even greater degree of reduction in H3K27me2/3. This level of sensitivity was previously undetectable in the western blot **(Figure 8A and 8B)**. There was an excellent agreement between western blot and flow cytometry results, but flow cytometry proved to be a superior method as it (1) allows single cell analysis (2) much higher level of sensitivity (3) greater time efficiency. Going forward we decided that given the numerous advantage of flow cytometry, that we would use this assay to validate loss of H3K27me2/3 in cells expressing the K27M transgenes and AML patient samples.

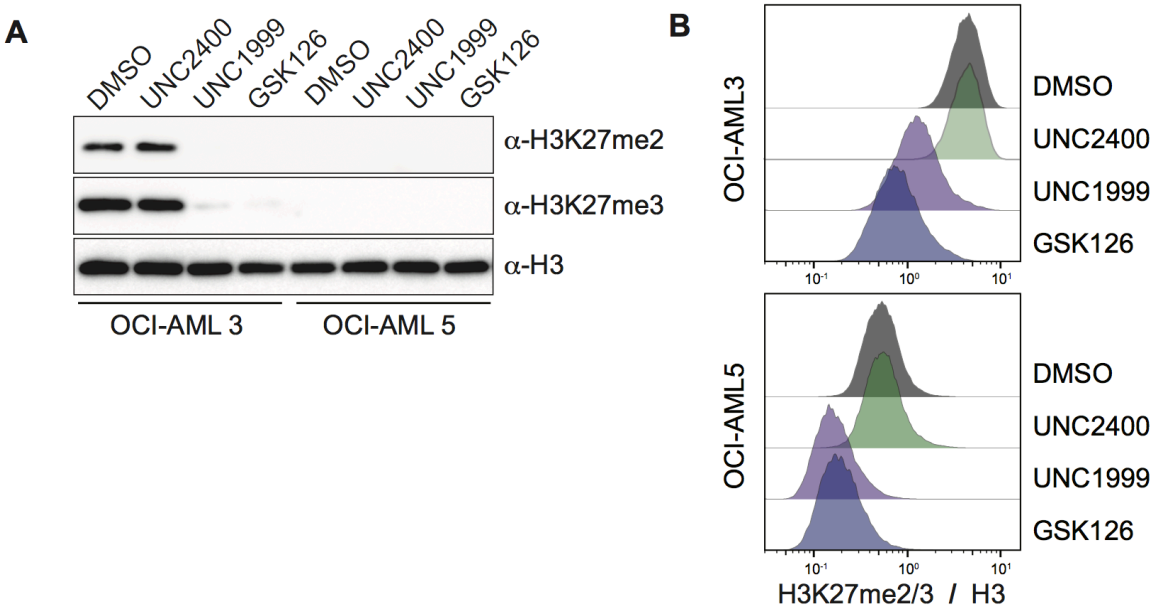

Figure 8. Flow cytometry is an effective tool to quantify H3K27me2/3 (A) Whole cell lysates of drug treated OCI-AML3 and OCI-AML5 (*EZH2*^{R690H}). Cells were treated with

drug vehicle (DMSO), inactive EZH inhibitor (UNC2400) or EZH inhibitors (GSK126 and UNC1999) for 72 hours (B) Alternatively, OCI-AML3 and OCI-AML5 cells were also fixed in cold ethanol and processed through flow cytometry. The H3K27me2/3 signal was then normalized to the H3 signal.

2.1.2 Identification of *H3$^{K27M/I}$* Mutation in AML Patients

Of the 415 sequenced adult AML patients within the Leucegene cohort, we identified two patients that had a mutation on lysine 27 of histone H3. Patient 04H138 had a mutation on the *HIST1H3H* gene where lysine 27 was mutated into a methionine (*HIST1H3H^{K27M}*). Patient 12H183 had a mutation on the *HIST1H3F* gene where lysine 27 was mutated into isoleucine (*HIST1H3F^{K27I}*). Next generation sequencing revealed that the *H3.1^{K27M}* and *H3.1^{K27I}* mutations occurred at a variant allele frequency (VAF) of less than 50%, suggesting a minor hemizygous mutant sub-clone **(Figure 9a)**. Gene expression profiles revealed that the mutated H3.1 gene contributed to 27.8% of total canonical histone H3 gene expression in patient 04H138 and 4.4% of total canonical H3 gene expression in patient 12H183. Together, this suggested that both variants are present in different sub-stoichiometric levels in the chromatin incorporate pool of histone H3 **(Figure 9c)**. The somatic nature of the mutations was confirmed by sequencing of the matching DNA obtained from buccal swaps. While the *HIST1H3F^{K27I}* mutation was also detected in the normal tissue sample, other AML mutations were also identified indicating the likelihood of a contamination in the swap **(Figure 9b).** Furthermore, in The Cancer Genome Atlas (TCGA) cohort of 200 AML patient samples, one patient was identified with a *K27M* mutation on *HIST1H3D* (*HIST1H3D^{K27M}*) [38]. Overall the *H3.1$^{K27M/I}$* mutated histone occurs at a frequency of 0.05% (1/200), indicating the rareness of this mutation in adult AML. Mutation profiles of *H3.1$^{K27M/I}$* AML patients showed that the mutated histone was likely to co-occur with other epigenetic modifiers that were suggested to have an impact on H3K27me3 including *BCOR, ASXL1, AXSL2,* and *EZH2*. Interestingly each of these H3.1$^{K27M/I}$ AML patients contained a unique mutation that altered RUNX1, suggesting a genetic synergy between mutated RUNX1 and reduced H3K27me3 **(Figure 9d)**.

In glioma patients, $H3^{K27M/I}$ mutations were proceeded by a reduction in H3K27me3 [50], to assess methylation levels in the heterogeneous AML patient samples we utilized our newly developed flow cytometry assay. In the *HIST1H3H*^{K27M} patient specimen the reduction in H3K27me2/3 was detectable in approximately 50% of the cells, which was consistent with the *HIST1H3H*^{K27M} VAF of 27.9%. In the *HIST1H3F*^{K27I} AML patient specimen we did not observe a loss of H3K27me2/3 representative of the VAF of 41%, nonetheless a small population within the patient specimen exhibited a loss of H3K27me3 **(Figure 9e)**. The discrepancy of the H3K27me2/3 signal between the two patients can be partially explained by (1) the mutated histone allele being expressed at 27.6% in patient 04H138 compared to 4.4% in patient 12H183 **(Figure 9c)** and (2) *in vitro* data suggesting that $H3^{K27M}$ was the more potent inhibitor of EZH1/2 (49). To validate, the presence of the mutated histone within the low H3K27me2/3 population, we performed cell sorts of the high and low H3K27me3 population, followed by Sanger sequencing. As anticipated, the histone mutation occurred exclusively within the population exhibiting reduced methylation **(Figure 9f)**. Taken together, our data were the first to identify rare heterogeneous *H3.1*$^{K27M/I}$ mutations in adult AML that have a dominant-negative effect on H3K27me2/3.

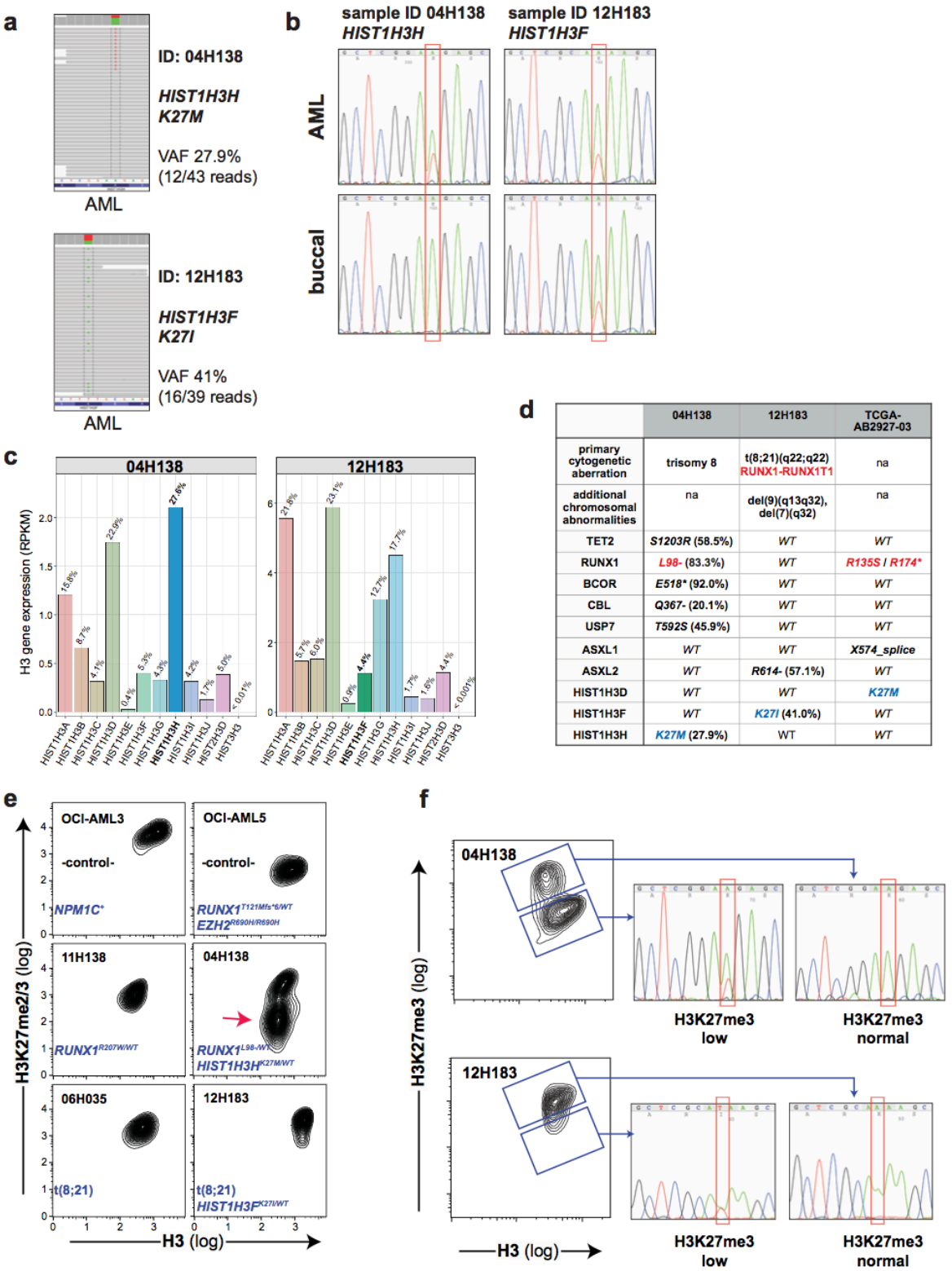

	04H138	12H183	TCGA-AB2927-03
primary cytogenetic aberration	trisomy 8	t(8;21)(q22;q22) RUNX1-RUNX1T1	na
additional chromosomal abnormalities	na	del(9)(q13q32), del(7)(q32)	na
TET2	*S1203R* (58.5%)	*WT*	*WT*
RUNX1	*L98-* (83.3%)	*WT*	*R135S* / *R174**
BCOR	*E518** (92.0%)	*WT*	*WT*
CBL	*Q367-* (20.1%)	*WT*	*WT*
USP7	*T592S* (45.9%)	*WT*	*WT*
ASXL1	*WT*	*WT*	*X574_splice*
ASXL2	*WT*	*R614-* (57.1%)	*WT*
HIST1H3D	*WT*	*WT*	*K27M*
HIST1H3F	*WT*	*K27I* (41.0%)	*WT*
HIST1H3H	*K27M* (27.9%)	WT	*WT*

Figure 9. Oncogenic histones H3.1^{K27M} and H3.1^{K27I} identified in AML patients to occur at low frequencies (a) Within the Leucegene cohort containing 415 sequenced AML patients with diverse cytogenetics, only two patients were identified to contain either the histone *H3.1^{K27M}* or *H3.1^{K27I}* mutation. (b) Sanger sequencing validated somatic mutations in H3.1$^{K27M/I}$ AML patients. Genomic DNA from AML cells (top) and buccal swaps (bottom). The missense mutation is highlighted in the red box. (c) Level of each histone H3 gene contributing to the total canonical histone H3 expression. In patient 04H138 the *HIST1H3H^{K27M}* variant is present on the highest expressed H3 (27.6% of all *H3* genes, highlighted in bold). In patient 12H183, expression of the *HIST1H3F* gene constitutes 4.4% of total canonical histone H3. (d) Mutation profile of H3.1$^{K27M/I}$ AML patients. Each patient harbored additional mutations effecting epigenetic modifiers and unique mutations altering RUNX1 (e) A subpopulation of diseased cells from 04H138 had 10-fold less H3K27me2/3. Reduction in H3K27me2/3 was less prominent in 12H183. (f) As indicated in the blue box, cells from *H3.1$^{K27M/I}$* AML patients were sorted per low and high H3K27me3. Sorted population were processed through Sanger sequencing and revealed that the missense histone mutation occurred specifically in the sub-population expressing low H3K27me3.

2.1.3 Collaboration between H3$^{K27M/I}$ with AML1-ETO9a Accelerates Disease Progression

Closer examination of the molecular profile of AML patients harboring the *H3$^{K27M/I}$* mutation revealed that all three patients had a *RUNX1* gene alteration. The 04H138 (HIST1H3H^{K27M}) patient had a heterozygous truncation of *RUNX1* at L98-, 12H183 (HIST1H3F^{K27I}) patient carried the RUNX1-RUNX1T1 translocation and TCGA K27M (HIST1H3D^{K27M}*)* patient had biallelic point mutations on the *RUNX1* gene (**Figure 9d**). Overall this suggested that (1) H3K27 mutation associates with RUNX1^{mut} AML (2) H3K27 mutation were likely to be a secondary mutation that arise from RUNX1^{mut} AML. We hypothesized a leukemia-accelerating collaboration between *RUNX1* alterations and reduced H3K27me2/3.

To investigate, the collaboration between *RUNX1* and H3$^{K27M/I}$ mutations, *AML1-ETO9a* and the *MLL-AF9* fusion gene were individually transfected into HSPCs isolated from mouse bone marrow to engineer a murine AML cell line. The engineered AE9a and MLL-AF9

cells were infected with a panel of $H3.3^{KM}$ transgenes including: $H3.3^{WT}$, $H3.3^{K27I}$, and $H3.3^{K27M}$ **(Figure 10a).** The proliferation kinetics were monitored over several passages in a competitive assay. Initially, it appeared that there was no proliferative advantage in any of the conditions, however by passage 3 in $H3.3^{K27M}$ AE9a and passage 7 in $H3.3^{K27I}$ AE9a, the frequency of the tdTomato marked cells significantly accelerated, while simultaneously the $H3.3^{WT}$ tdTomato-marked cells continued to decline. More importantly, $H3.3^{WT}$, $H3.3^{K27I}$, and $H3.3^{K27M}$ all conferred a similar disadvantage in MLL-AF9 cultures **(Figure 10b)**. By the end of passage 10 it was clear that AE9a expressing $H3.3^{K27M/I}$ that had originally occupied ~70% of the culture had proliferated to dominate the culture as shown by the strong transgene expression **(Figure 10c).** H3K27me3 levels were validated through flow cytometry and showed that $H3.3^{K27I/M}$ infected AE9a cells exhibited significant reductions in H3K27me2/3 signal relative to $H3.3^{WT.}$ **(Figure 10d).** Together, these results demonstrated that expression of $H3.3^{K27I}$ and $H3.3^{K27M}$ synergized with AE9a but not MLL-AF9 AML cells *in vitro*.

To further validate our hypothesis that $H3.3^{K27I}$ and $H3.3^{K27M}$ confer a selective proliferation advantage to AE9a but not MLL-AF9 AML, the engineered murine leukemia cells expressing $H3.3^{WT}$, $H3.3^{K27I}$ or $H3.3^{K27M}$ were transplanted into mice recipients **(Figure 10e)**. The first mice to reach disease end stage were AE9a driven AML expressing $H3.3^{K27M,}$ $H3.3^{K27I}$ and then followed by $H3.3^{WT}$ much later. This demonstrated a clear acceleration of disease development in the $H3.3^{K27M/I}$ mice compared to $H3.3^{WT}$ in AE9a AML **(Figure 10f)**. Histological analysis from bone marrow isolated from the diseased leukemic AE9a mice showed an accumulation of characteristic AML blast cells. Furthermore, histological analysis of livers and spleens displayed a high infiltration of leukemic cells indicative of full-blown AML pathologies **(Figure 10h)**. All diseased recipients contained a high fraction of c-Kit positive cells characteristic of AML blasts in this model. Isolated leukemic bone marrow cells contained readily discernible cell populations with largely decreased H3K27me2/3 levels specific to the $H3.3^{K27I}$ and $H3.3^{K27M}$ groups **(Figure 10i).** In contrast, MLL-AF9 expressing $H3.3^{K27I/M}$ did not experience changes in disease latencies compared to the control group **(Figure 10g)**. This reiterated our previous conclusion that in the context of AML1-ETO9a-driven leukemia, H3K27me3 acts as a tumour suppressor. Notably, the more potent inhibitory effect of the

H3.3^{K27M} mutant on PRC2 compared to H3.3^{K27I} resulted in a stronger cooperation with AE9a demonstrating that varying degrees of PRC2 inhibition have quantitatively different effects on leukemia progression in t(8;21) AML.

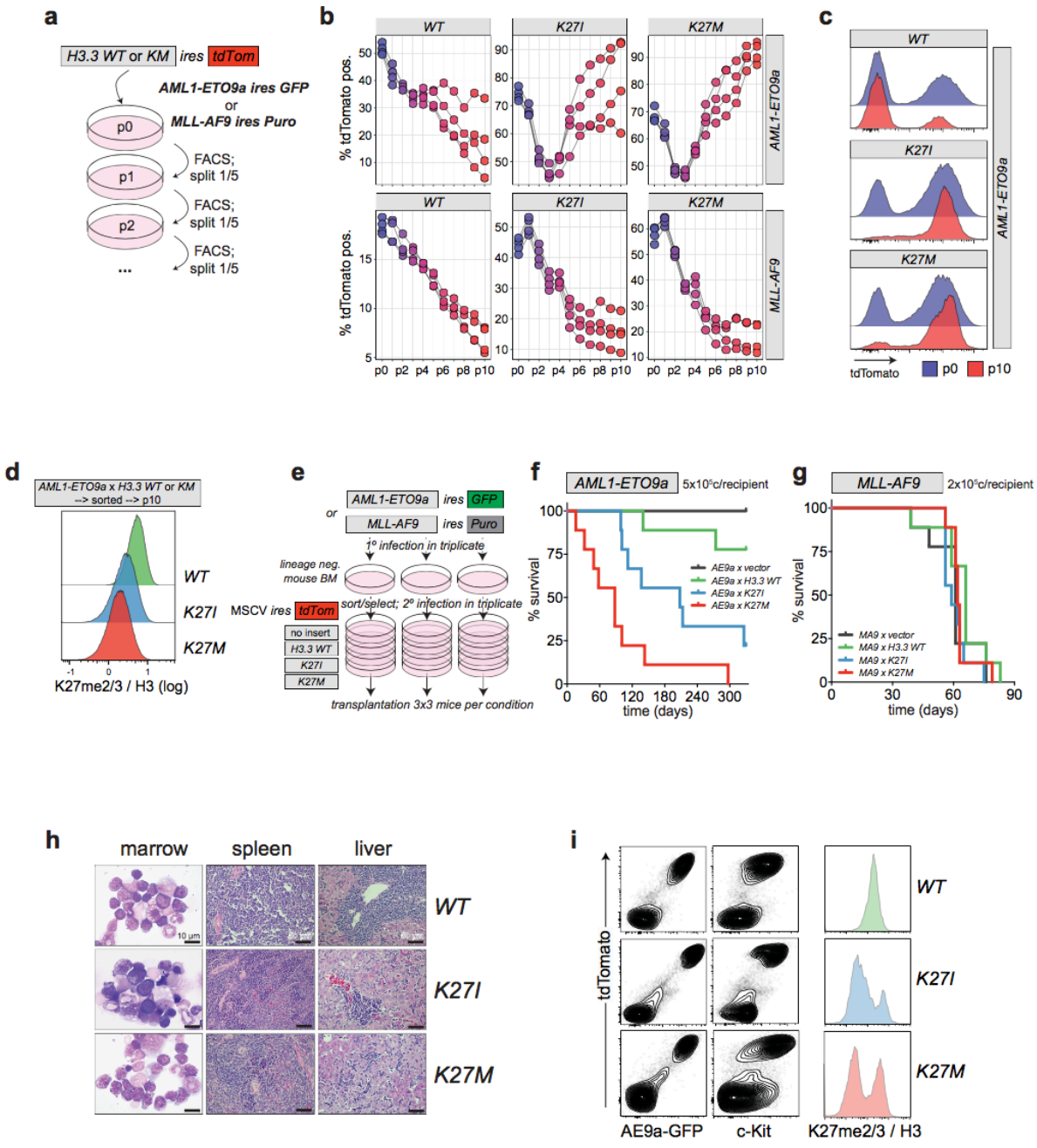

Figure 10. Collaboration between H3.3K27I/M and AML1-ETO9a (AE9a) accelerated disease development. (a) Experimental strategy of competitive in vitro cellular proliferation

assays to examine AML1-ETO9a or MLL-AF9 immortalized mouse bone marrow cells with MSCV H3.3^{KM} mutants IRES tdTomato. Cellular proliferation was measured by monitoring percentage tdTomato over several passages using flow cytometry (b) Transformed AML1-ETO9a or MLL-AF9 cells expressing the H3.3^{KM} mutants were passaged 10 times to reveal cell proliferation activity. (c) Histogram representation tdTomato FACS profiles at passages 0 and 10 indicate selection for high expression of H3.3$^{K27I/M}$ at the end of the culture period in AE9a cells. (d) Histogram representation of global H3K27me2/3 normalized to H3 signal. AML1-ETO9a cells expressing the H3.3$^{K27M/I}$ were sorted on tdTomato positivity and passaged 10 times. (e) Experimental strategy to assess AML progression upon H3.3^{KM} expression in vivo. (f-g) Survival curves of mice transplanted with $5*10^5$ AML1-ETO9a or $2*10^5$ MLL-AF9 cells expressing the H3.3$^{K27M/I}$ mutants. (h) Pathological analysis of diseased AE9a cell recipients indicates typical AML end-stage characteristics. Bone marrow cells collected from disease mice showed a selection for cells expressing high level H3K27M marked by tdTomato and c-Kit. H3K27M/I mice exhibited a reduction of H3K27me2/3.

2.1.4 H3K27me2/3 in RUNX1 altered AML Patients

EZH2 mutations occurred almost exclusively in the context of *RUNX1* mutations in AML (either RUNX1-RUNX1T1 or RUNX1^{mut}). This suggested further epigenetic instability from *EZH2* mutations may be required to complement *RUNX1* mutated patients. Hence, we hypothesized that *RUNX1* altered AML may express lower levels of H3K27me3 compared to *RUNX^{WT}* AML. This prompted us to further investigate H3K27me2/3 in primary AML patients with *RUNX1* alterations. To this end, we examined H3K27me2/3 in 29 AML patient samples, our panel included: 13 control patients, 10 patients with t(8;21)(q22;q22) translocation and 6 patients with mutations in the *RUNX1* gene. 5,000 single cell events were examined from each of the described patients. Our result indicated that with the exception of the H3.1$^{K27M/I}$ patient no other patient sample exhibited any significant reduction in H3K27me3 that was detectable by flow cytometry **(Figure 11)**. However, it should be mentioned that flow cytometry has limited detection compared to ChiP-sequencing (ChiP-seq).

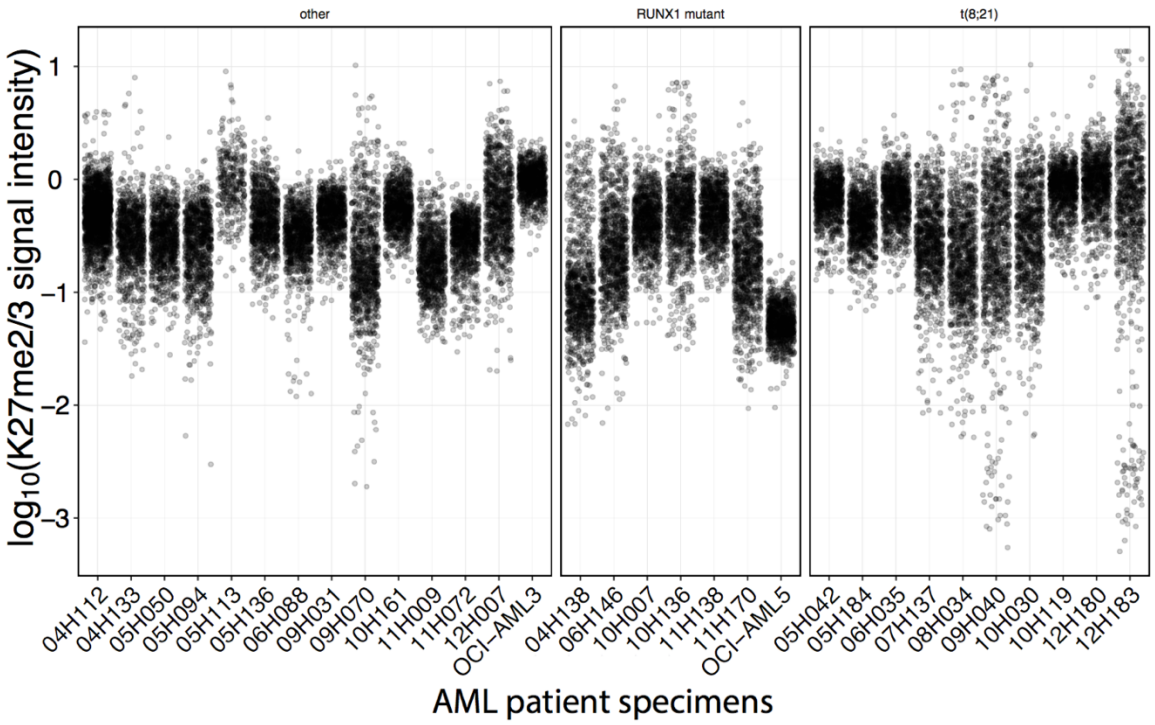

Figure 11. Quantification of global H3K27me2/3 in AML patient specimens. 5,000 single cell events representing the level of H3K27me2/3 in AML patients specimens were acquired through flow cytometry in RUNX1^{mut}, t(8;21) and control patient specimens.

From transcriptome data of Leucegene patients, we examined differentially expressed genes in RUNX1^{mut}, t(8;21) and RUNX1^{WT} AML patients, the primary aim was to assess if there were any indications that H3K27me3 was hindered in patients harboring a defective *RUNX1* gene. Comparative transcriptomic analysis revealed there was a decrease in expression of components of PRC2 including EED and SUZ12 in t(8;21) patients, that would suggest a decrease in H3K27me3 **(Figure 12)**. In summary, there was no clear loss of H3K27me2/3 in RUNX1 altered patients other than the histone H3.1$^{K27M/I}$ patients previously described. However, t(8;21) AML patients have decreased expression of PRC2 components, that could suggest reduced levels of H3K27me3 that was not detectable through flow cytometry.

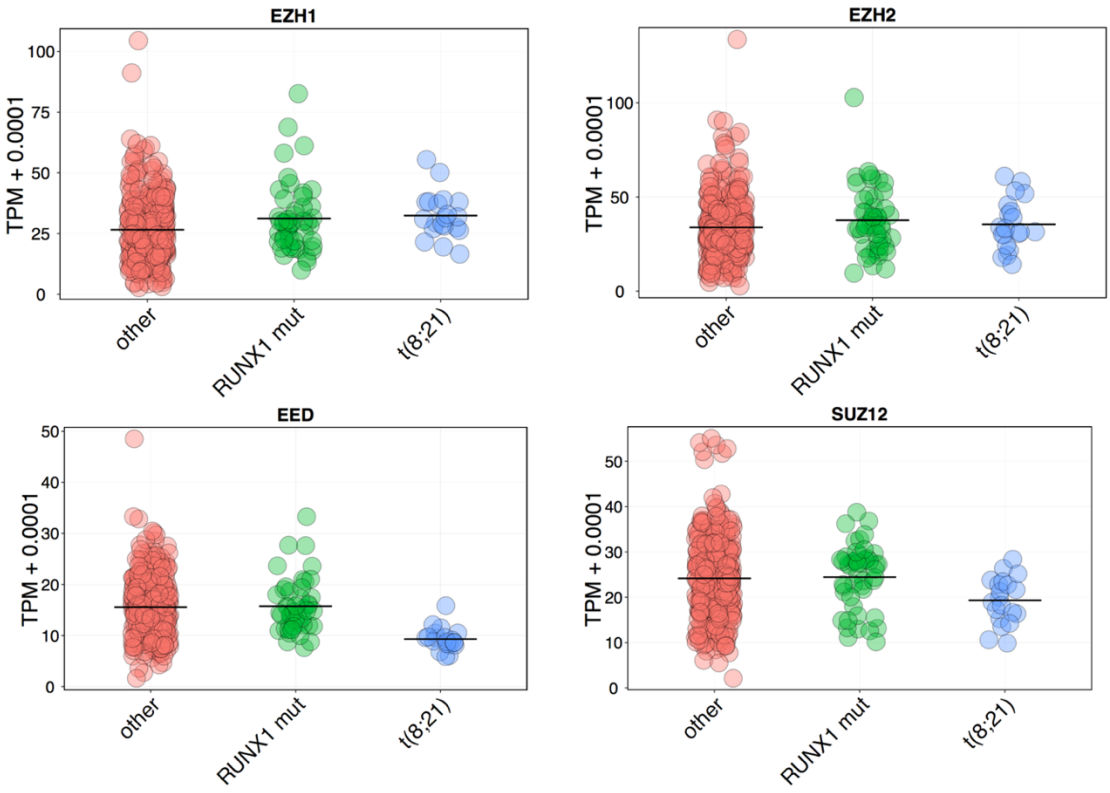

Figure 12. Low expression of core PRC2 members in t(8;21) AML. Transcriptome analysis of core components of PRC2 in patients categorized based on RUNX1 mutation status into RUNX1^{mut,} t(8;21) and other (i.e. RUNX1^{WT}) group. Significant reduction in expression of EED and SUZ12, but not EZH1/2 was observed in t(8;21) AML.

2.2 Functional Investigation of H3^{K27M} in Normal Hematopoiesis

2.2.1 Reduction of H3K27 Methylation Selectively Expands Human Progenitor Population

To investigate the influence of H3K27 methylation on differentiation, self-renewal and proliferation of human HSPCs, we infected cells with lentivirus expressing the H3.3^{KM} mutants. The lentiviral constructs included the no insert (i.e. empty vector), *H3.3*^{WT}, *H3.3*^{K9M} *and H3.3*^{K27M} mutant followed by an *IRES GFP* cassette. These cells were maintained in optimized HSC expansion conditions that contained the small molecule UM171 [66]. By western blot analysis, we observed a global reduction of H3 methylation on the corresponding lysine marks

in lentiviral infected HSPCs. For instance, expression of H3.3^{K27M} reduced global H3K27me2/3 **(Figure 13a)**. At day 10, we examined the surface phenotype of the expanded cells and detected striking surface phenotype changes on HSPC expressing H3.3^{K27M}. Specifically, these cells maintained higher frequencies of primitive CD34^{+}/CD45RA^{-} cells compared to all other tested conditions (empty vector, H3.3^{WT} and H3.3^{K9M}). A more detailed analysis revealed that expression of H3.3^{K27M} led to the eightfold expansion of a CD34^{+}/CD45RA^{-}/CD90^{+}/CD133^{-} population and a mild expansion of a CD34^{+}/CD45RA^{-}/CD90^{+}/CD133^{+} population. The expansion of the CD133^{-} population indicated to us that H3.3^{K27M} infected HSPCs had expanded a progenitor population and not an HSC population **(Figure 13b and 13c)**.

We hypothesized that H3.3^{K27M} mediated expansion of the described progenitor population was due to the loss of H3K27me2/3. Therefore, inhibiting the methyltransferase activity of EZH1/2 should mimic the H3.3^{K27M} phenotype. As predicted, pharmacological inhibition of EZH1/2 not only ablates the presence of H3K27me2/3, but can expand the CD34^{+}CD45RA^{-} CD90^{+} population in a dose dependent manner. The treated cultures reached the absolute maximal expansion of CD34^{+}/CD45RA^{-}/CD90^{+} cells at 1μm. At this concentration, this was accompanied by an almost 50% reduction in total cell numbers in the same cultures, suggesting that although pharmacological inhibition of EZH1/2 augments the expansion of CD34^{+}/CD45RA^{-}/CD90^{+} cells, its impact on the remainder of the culture is detrimental **(Figure 13d and 13e)**.

Given that H3.3^{K27M} reduces methylation through the inhibition of EZH1/2 [50], we hypothesized that the expression of H3.3^{K27M} and EZH1/2 inhibition likely expanded CD34^{+}/CD45RA^{-}/CD90^{+} cells through the same mechanism (the loss of H3K27me2/3). To validate this hypothesis, we exposed HSPCs infected with the *H3.3^{KM}* lentiviral constructs to either DMSO, GSK126, UNC2400 or UNC1999 at 1μM. The combination of H3.3^{KM} expression with GSK126 or UNC1999 treatment led to a similar expansion of the CD34^{+}/CD45RA^{-}/CD90^{+}/CD133^{-} population in all lysine-to-methionine culture conditions (vector only, *H3.3^{WT}*, *H3.3^{K9M}*, *H3.3^{K27M}*) (**Figure 13f**).

In summary, the data demonstrated that the expression of H3.3^{K27M} caused a marked reduction of H3K27me2/3 and led to profound phenotypic changes in primitive human hematopoietic cells. Given the strikingly similar phenotypical effect of H3.3^{K27M} expression and EZH1/2 inhibition on these cells, the effect of H3.3^{K27M} on human HSPCs is likely prompted by its inhibition of EZH1/2.

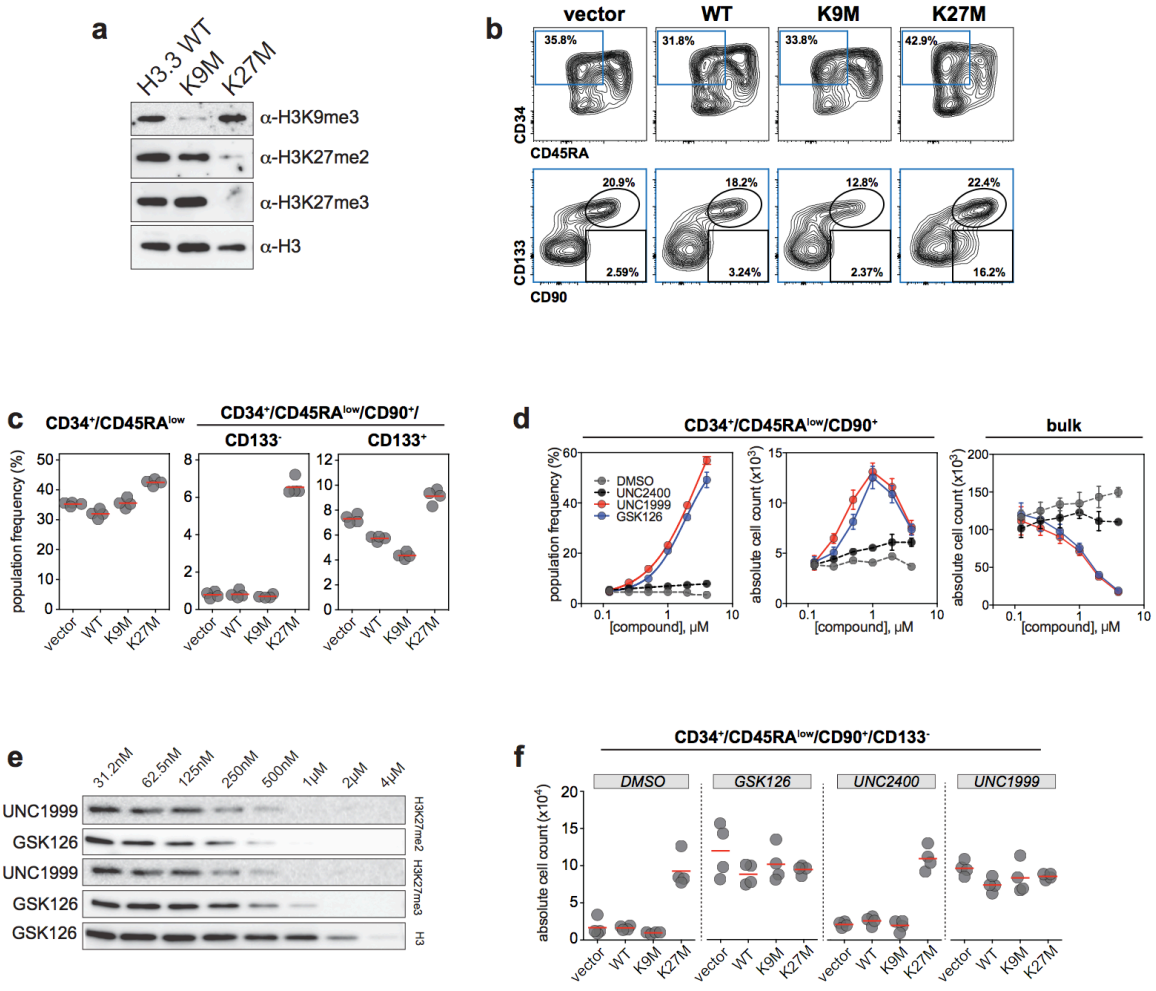

Figure 13. Reduction of H3K27me2/3 expands a selective human progenitor population

(a) Modification of histone marks by H3.3^{KM} mutant expression were analyzed by western blot using whole cell lysates. Efficient decrease in H3K27me2/3 or H3K9me3 from expression of H3.3^{K27M} or H3.3^{K9M}. (b) Phenotypic characterization of H3.3^{KM} mutants expressed in human HSPC, and cultured for 10 days. Presentation of flow cytometry gating

strategy to analyze subpopulations. Gated on the $CD34^+CD45^-$ subpopulation followed by gating into either $CD90^+/CD133^-$ or $CD90^+/CD133^+$. Percentage of each gated subpopulation is represented. (c) Summary of population frequency of subpopulations. HSPCs expressing $H3.3^{K27M}$ displayed a selective expansion of the $CD34^+/CD45RA^-/CD90^+/CD133^-$ population and a mild increase in the $CD34^+/CD45RA^-/CD90^+/CD133^+$ population. (d) Dose-dependent increase in the percentage of $CD34^+/CD45RA^-/CD90^+$ cells (left panel) in EZH1/2 inhibitor treated HSPCs. Expansion of $CD34^+/CD45RA^-/CD90^+$ cells in absolute cell numbers (middle panel). Absolute cell numbers in total culture (right panel) (e) Dose-dependent decrease of H3K27me2/3 in EZH1/2 inhibitor treated HSPCs. EZH1/2 inhibitor treated cultures from (d) were pooled and used for Western blot analysis using the indicated antibodies. (f) All $H3.3^{KM}$ HSPCs treated with EZH1/2 inhibitors(1μM) led to a similar fold-expansion of the $CD34^+/CD45RA^-/CD90^+/CD133^-$ population. Cells were analyzed at d10 post-infection and EZH1/2 inhibitor treatment.

2.2.2 shRUNX1 phenocopies immunophenotype of $H3.3^{K27M}$

Based on our previous observation that $H3.3^{K27I}$ or $H3.3^{K27M}$ exhibited a genetic synergy with *AML1-ETO9a* mouse model of t(8;21) AML, we hypothesized that hindering RUNX1 expression in human HSPCs could mimic the expansion of the $CD34^+/CD45RA^-/CD90^+/CD133^-$ population previously seen in HSPCs expressing $H3.3^{K27M}$. To validate this hypothesis, we designed shRNAs targeting RUNX1. Knockdown was validated using western blot analysis and showed a 50-80% decreased expression of the RUNX1 protein **(Figure 14a)**. When surface phenotype was examined at d10, we observed a knockdown dependent expansion of $CD34^+/CD45RA^-/CD90^{+/}CD133^-$ cells and to a much lesser extent a mild expansion of the $CD34^+/CD45RA^-/CD90^+/CD133^+$ cells in HSPCs **(Figure 14b)**. These results mimicked the changes in the surface phenotype that we had observed in HSPCs expressing $H3.3^{K27M}$. Overall, it highlighted the importance of further investigating the mechanisms governing the genetic synergy between the loss of RUNX1 and hypo-H3K27me2/3.

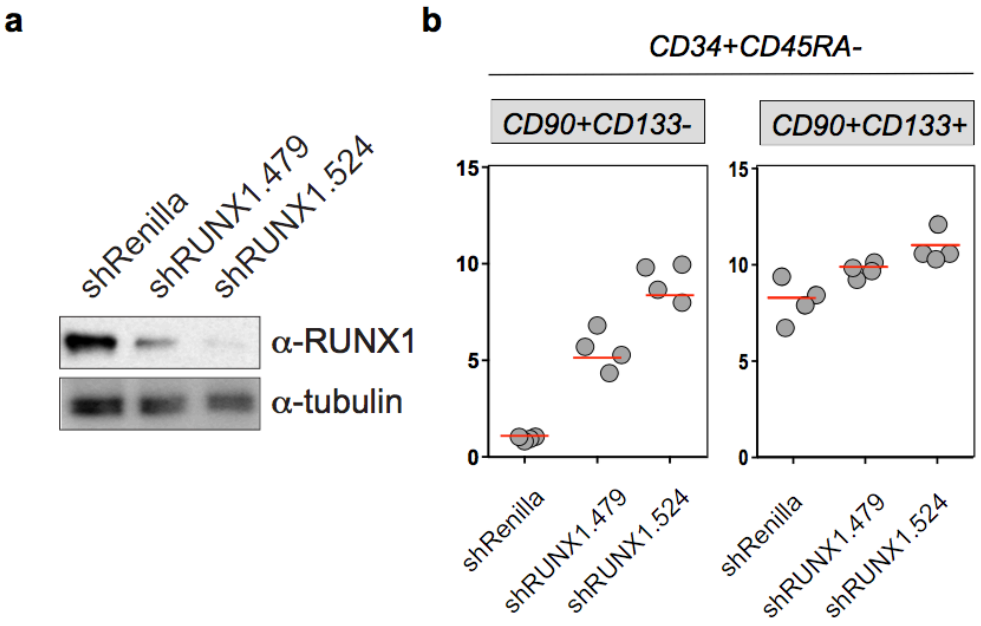

Figure 14. shRUNX1 mimics H3.3^{K27M} in the expansion of CD34+/CD45RA-/CD90+/CD133- (a) Lentiviral expression of shRUNX1 induces a specific reduction in RUNX1 expression in cultured human HSPCs as shown by western blot analysis. (b) Phenotypic characterization of HSPCs expressing shRUNX1. CD34^{+} cells derived from UCB were infected with lentivirus expressing shRUNX1 and cultured for 10 days. A similar gating strategy as previously described was applied, and revealed that knockdown of RUNX1 mimicked H3.3^{K27M} in its ability to expand the progenitor CD34+/CD45RA-/CD90+/CD133- population.

2.2.3 *H3.3^{K27M}* Expression Enhances the Activity of Committed Myeloid Progenitors and Results in Mild Loss of LT-HSC Self-renewal

To delineate the HSPC differentiation stages that were modulated by H3.3^{K27M}, we first maintained empty vector control, H3.3^{WT}, H3.3^{K9M} or H3.3^{K27M} infected human HSPC cultures ex vivo for 14 days and plated equal numbers of GFP^{+} cells into methylcellulose media to assess their clonogenic potential. Strikingly, we observed increased numbers of unipotent mature colonies that were granulocytic and granulo-monocytic but not multipotent immature colonies (granulo/erythroid/monocytic/megakaryocytic; GEMM) colony forming cells upon expression of H3.3^{K27M} compared to control and H3.3^{K9M} conditions **(Figure 15)**.

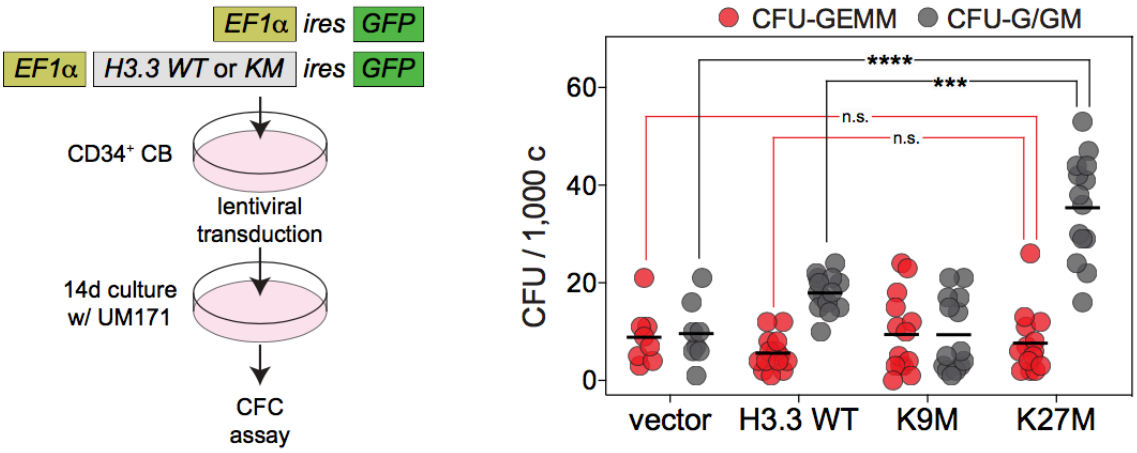

Figure 15. *H3.3*^{K27M} expression enhances the activity of committed myeloid progenitors. Assessment of myeloid progenitor activity in response to *H3.3*^{K27M} expression. Human HSPCs were infected with lentiviral particles and cultured in UM171-containing HSC-supporting conditions for 14 days. GFP^{+} cells were FACS sorted and plated in methylcellulose media supporting erythro-myeloid differentiation. Colonies were morphologically assessed and scored after 14 days. Combined results from two independent experiments are presented. Granulo-erythoid-monocyte-megakaryocyte colony-forming units (CFU-GEMM) and granulo/granulo-monocyte colony-forming units (CFU-G/GM) were scored.

To investigate the self-renewal and differentiation capacity of H3.3^{KM} HSCs, we performed a series of classical competitive transplantation experiments. LT-HSCs were isolated through the c-Kit^{+}Lin^{-}Sca1^{+}CD150^{+}CD244^{-}CD48^{-} (KLS-SLAM) immunophenotyping and infected with retroviruses expressing the mutant version of H3.3^{KM}. The retroviral *IRES GFP* constructs included the no insert (ie. empty vector), *H3.3*^{WT} or *H3.3* mutant (*K9M* or *K27M)*. After 5 days of *in vitro* culture in BM media, infected LT-HSCs and helper BM cells were transplanted into lethally irradiated mice recipients. HSC self-renewal and multilineage reconstitution activity were monitored through infected GFP^{+} cells in the peripheral blood **(Figure 16a).** At 4 weeks, the GFP^{+} population reflected the activity of short-term HSCs and progenitor populations. At this point, H3.3^{K27M} donor cells showed good engraftment potential, no detrimental effect on short term reconstitution and no lineage

biases. After 24 weeks of engraftment, mice in the H3.3 ^{K27M} group appeared to have a mild loss of HSC activity as demonstrated by the loss of GFP+ cells over time, but still showed no lineage bias (**Figure 16b and 16c)**.

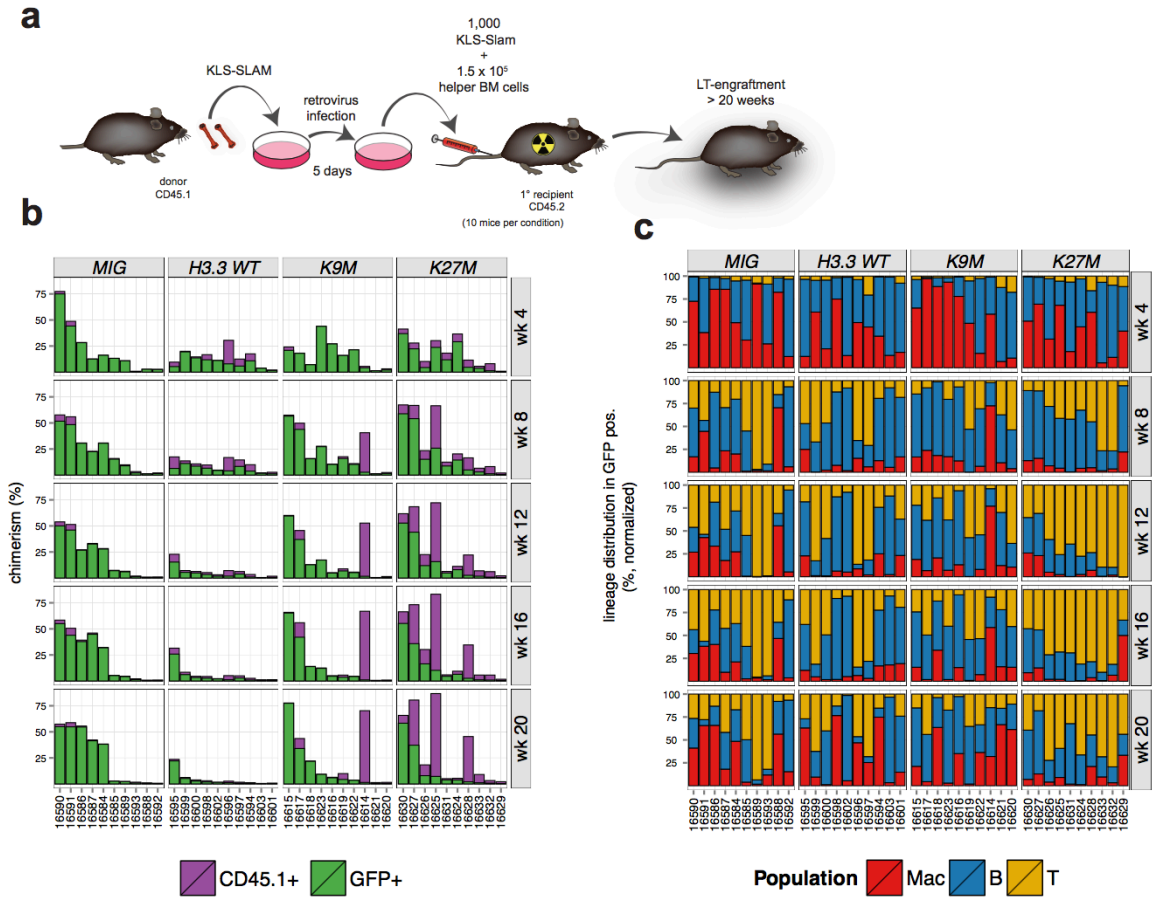

Figure 16. Reduction of H3K27me2/3 has a mild impact on mice LT-HSC (a) Experimental strategy to assess HSC function in cells expressing H3.3^{KM}. Bone marrow from CD45.1 mice was extracted and enriched for the LT-HSC population using the KLS-SLAM phenotype. The KLS-SLAM HSCs were infected with retroviruses expressing H3.3 ^{KM} mutants. Infected cells were cultured for 5 days. Subsequently, 10^3 KLS-SLAM cells and 1.5 x 10^5 helper BM cells were transplanted into 10 CD45.2 recipient mice/condition. (b) Summary of histone H3.3^{KM} mutant on HSC expansion/engraftment. Peripheral blood chimerism of recipient CD45.2 individual mice were determined by FACs on the basis of

GFP and CD45.1 surface expression levels of individual mice at 4, 8, 12, 16 and 20 weeks post-transplantation. Individual mouse IDs are indicated at the bottom of the graph. (c) The presented data refers to the distribution of B, T and Mac cells within in the GFP^+ compartment.

Similarly, we performed *in vivo* transplantation experiments using human HSPC cells infected with lentivirus expressing the same panel of $H3.3^{KM}$ as previously described. Infected cells were cultured in UM171-containing HSC expansion media for 10 days and the outcome of 10^4 HSPCs were transplanted into NSG recipient mice **(Figure 17a).** At 4 weeks post transplantation, $H3.3^{K27M}$-infected HSPCs contributed less efficiently to short-term engraftment compared to control and the $H3.3^{K9M}$ conditions. Importantly, at 24 weeks there was no change in HSC activity observed in $H3.3^{K27M}$ versus empty vector or $H3.3^{WT}$ infected conditions, but lineage distribution presented mice with mild myeloid expansion. Taken together, the data indicated that expression of $H3.3^{K27M}$ potentiates the limited self-renewal capacity of committed myeloid progenitors *in vitro* but only mildly favors myeloid distribution *in vivo* and has no impact on human LT-HSC self-renewal. Notably, $H3.3^{K9M}$ mice showed an increased frequency of $CD33^+$ cells leading us to conclude that loss of H3K9me3 may lead to myeloid expansion. This observation was outside the scope of my thesis but could merit further investigation in the future. **(Figure 17b and 17c)**.

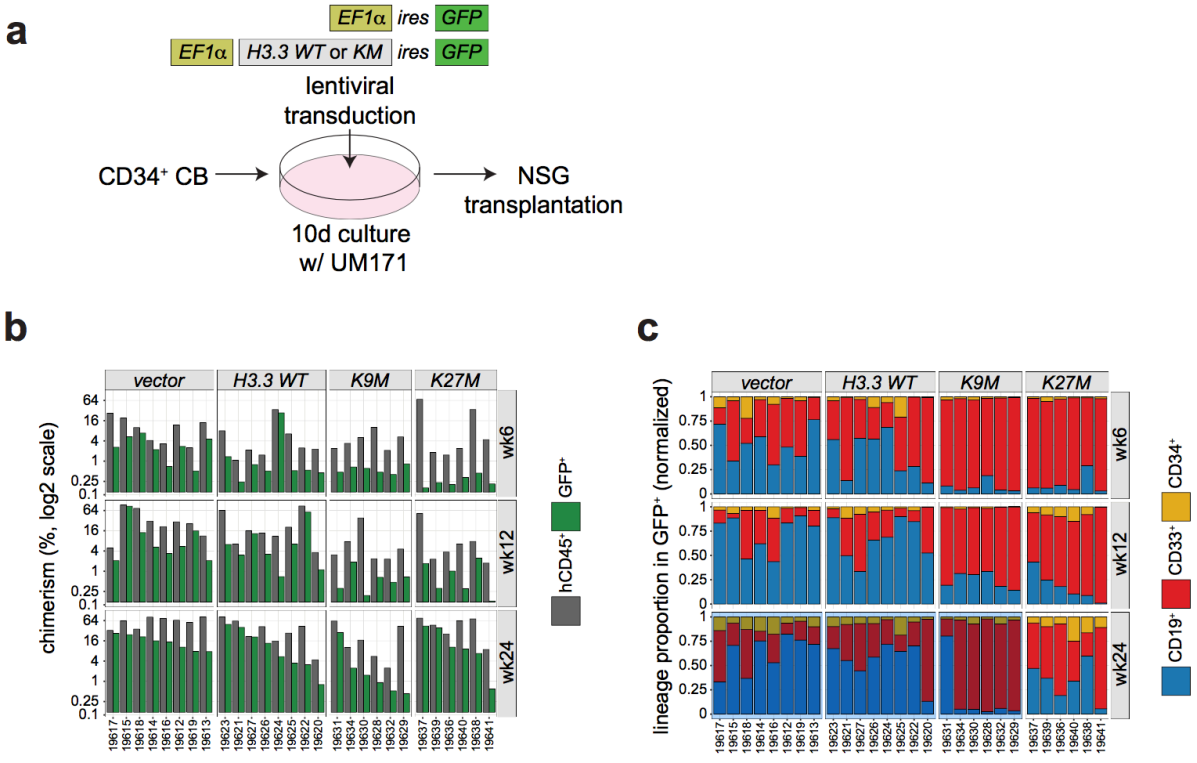

Figure 17. Reduction of H3K27me2/3 has a mild impact on human LT-HSC (a) Experimental strategy for *in vivo* transplantation of human HSPCs expressing H3.3^{KM} mutants. HSPCs were infected with lentivirus expressing H3.3^{KM} mutants and cultured for 10 days in the presence of UM171. Proceeding expansion, the outcome of approximately 10 colony forming units (CFU) were transplanted into 8 mice/condition. (b) Summary of total human cells and GFP+ engraftment of individual mice at week 6, 12 and 24. Bone marrow chimerism of transplanted NSG mice was determined by FACS-analysis based on GFP+ and human CD45 surface expression at the specified post-transplantation time-points. (c) Lineage distribution of HSPCs expressing *H3.3^{KM}* in transplanted NSG recipient mice. The presented data refers to the distribution of myeloid (CD33), B-lymphoid (CD19) and immature (CD34) surface phenotypes within the GFP^{+} compartment. Individual mouse IDs are indicated at the bottom of the graph.

To more indefinitely conclude the effect of reduced H3K27me2/3 on HSC function we performed a limiting dilution assay (LDA). Human HSPCs were treated with EZH inhibitors

(GSK126 and UNC1999) and controls (UNC2400 and DMSO) in the presence of UM171 in a fed batch culture [61]. Proceeding 10 days of *in vitro* expansion, we transplanted the outcome of 10, 2 or 0.5 colony forming unit (CFU) into NSG mice **(Figure 18a)**. After 24 weeks *in vivo*, limiting-dilution analysis demonstrated that both EZH1/2 inhibitors (GSK126 and UNC1999) negatively affected HSC expansion leading to an approximately 2-fold reduction in LT-HSC expansion. This suggested that the loss of H3K27me2/3 through the inhibition of EZH1/2 has a detrimental effect on HSPCs (**Figure 18b-g**).

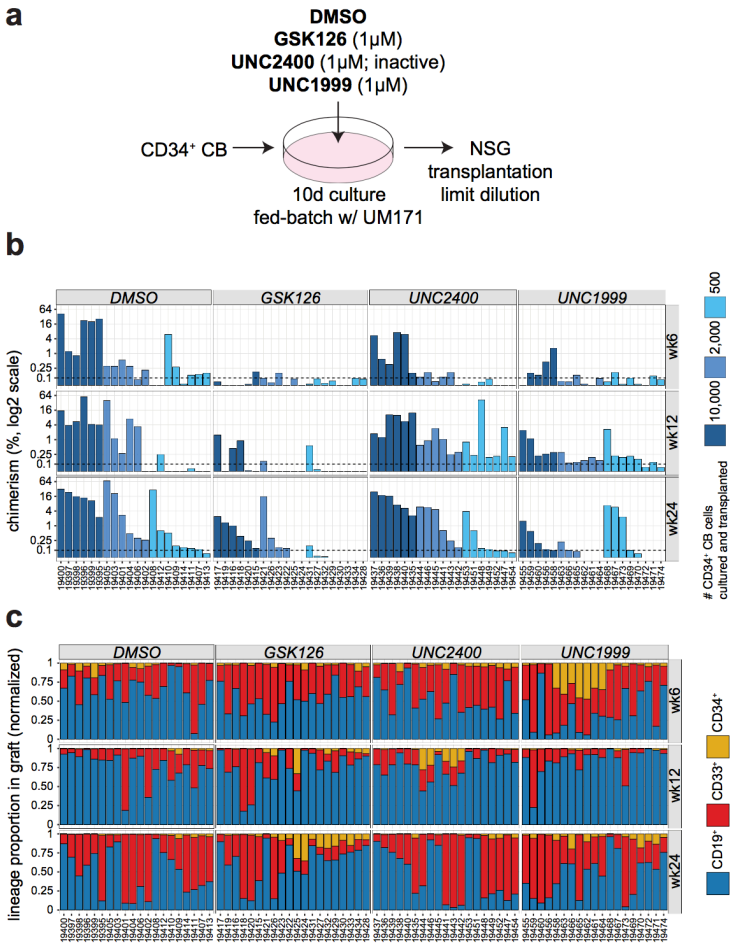

d

	positive recipients			
Cell Dose	DMSO	UNC2400	UNC1999	GSK126
10^5	6/6	6/6	4/5	6/6
$2x10^3$	6/6	6/6	2/6	4/6
$5x10^2$	7/8	4/7	4/8	1/8

e

	HSC frequencies (based on d0 input cell dose)			
	DMSO	UNC2400	UNC1999	GSK126
Lower CI	1/575	1/1,162	1/7,562	1/4,626
Estimate	1/240	1/520	1/3,419	1/2,116
Higher CI	1/100	1/233	1/1,546	1/968

f

	Absolute Cell Number Transplanted			
Cell Dose	DMSO	UNC2400	UNC1999	GSK126
10^5	1,272,917	737,789	248,471	355,064
$2x10^3$	254,583	147,558	49,694	71,012
$5x10^2$	63,646	36,889	12,424	17,753

g

	HSC frequencies (based on transplanted cell dose)			
	DMSO	UNC2400	UNC1999	GSK126
Lower CI	1/73,120	1/85,729	1/187,904	1/164,266
Estimate	1/30,533	1/38,368	1/84,949	1/75,147
Higher CI	1/12,750	1/17,171	1/38,405	1/34,378

Figure 18. Limiting Dilution Assay assessing HSC frequency (a) Experimental strategy to assess *ex vivo* HSPC-expansion in the presence of EZH1/2 inhibitors. HSPC expanded in fed batch culture with UM171, in addition to treatment with either drug vehicle (DMSO), inactive (UNC2400) or active EZH1/2 inhibitors (UNC1999 and GSK126) for 10 days (b)

Summary of total human CB engraftment for 10^4, $2*10^2$ or $5*10^2$ CRU of transplanted cells. Individual mice were assessed for engraftment at week 6, 12 and 24. Individual mouse IDs are indicated at the bottom of the graph. c) Lineage differentiation within human graft. (d) Number of positively engrafted mice (hCD45> 0.1%) (e) Estimate HSC frequencies calculated using CFU transplanted demonstrated a decrease with EZH inhibitor treatment. (f) Absolute number of cells transplanted after 10 day expansion. (g) Estimate HSC frequencies calculated using absolute number of cells transplanted, demonstrated decrease HSC frequency with EZH inhibitor treatment.

2.3 Investigation of Targeted Therapy for RUNX1 altered AML Patients

2.3.1 t(8;21) and *RUNX1* mutant AMLs are sensitive to H3K27 demethylase inhibition.

Given that reduced H3K27me2/3 had accelerated disease progression in *RUNX1* translocated AML, we predicted a possible sensitivity to pharmacological inhibition of the H3K27-specific demethylases UTX and JMJD3 in these AMLs. To test this hypothesis, we investigated the responses of a collection of genetically diverse human AML cell lines to the UTX/JMJD3 inhibitor GSK-J4 or its isomeric control drug GSK-J5 [43]. *RUNX1-RUNX1T1* translocation (Kasumi1 and SKNO1) or a truncating heterozygous mutation in *RUNX1* (OCI-AML5) were exposed to varying concentration of GSK-J4 (0.5-2.5 μM) for 72 hours. Exposure to 2.5 μM GSK-J4 for 72 hours elicited a strong anti-proliferative apoptotic response in cell lines carrying either the $RUNX1^{mut}$ or *RUNX1-RUNX1T1*. Apoptosis induction and a substantial reduction in live cell numbers were consistently observed in these cell lines when exposed to established effective doses of 1-2.5μM of GSK-J4. Importantly, treatment with GSK-J5 had no discernible effect on the survival and proliferation of these cells and was not distinguishable from untreated controls, demonstrating specificity of action. Moreover, OCI-AML2 cells and most other tested *RUNX1* WT AML cell lines (with the exception of KG1a) were insensitive to GSK-J4 and exhibited unchanged apoptosis and proliferation parameters compared to untreated or GSK-J5 treated controls. Taken together, these results demonstrate that sensitivity to H3K27-

demethylases inhibition by GSK-J4 represents a selective and potent vulnerability in AMLs with *RUNX1* gene alterations.

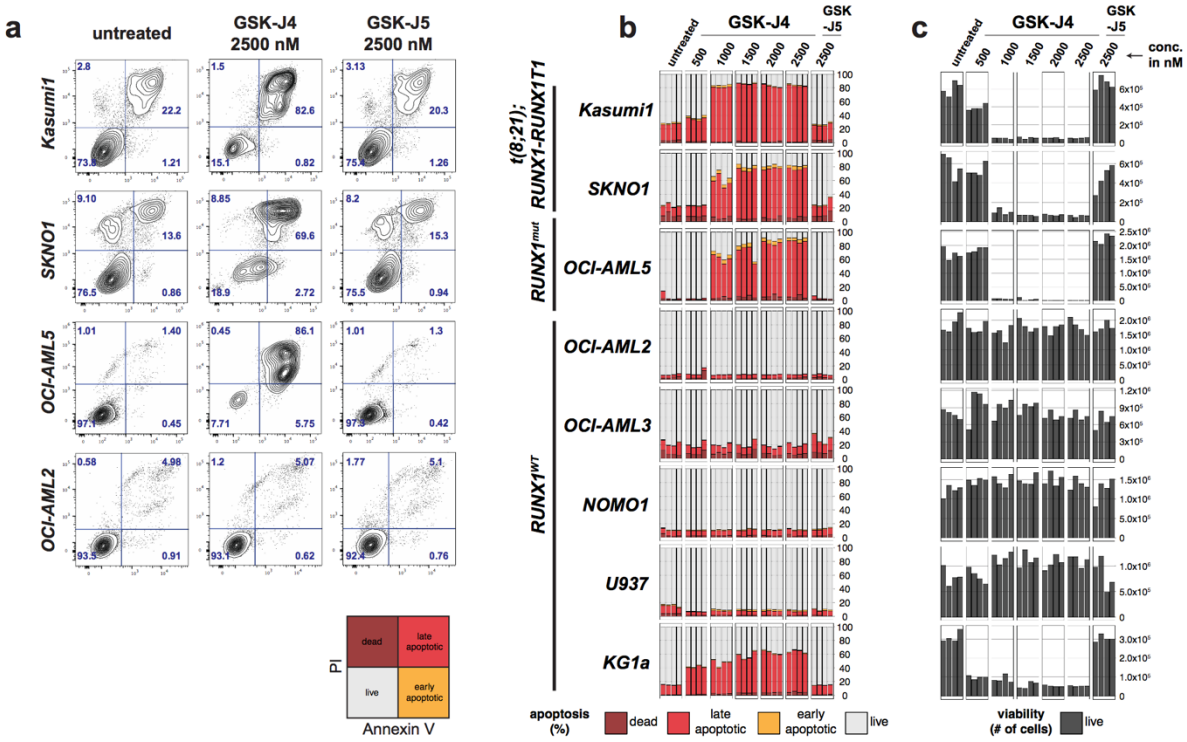

Figure 19. Selective sensitivity of t(8;21) and *RUNX1*^{mut} AML cell lines towards H3K27 demethylase inhibitor GSK-J4. (a) FACs representation of apoptosis induction in AML cell lines carrying the t(8;21) translocation or mutation in *RUNX1*. Cells were either left untreated or treated with 2.5 µM GSK-J4 or 2.5 µM GSK-J5(inactive control) for 72h, harvested and analyzed by Annexin V and propidium iodide staining. (b) Complete summary of apoptosis studies. Four replicates are plotted, cell lines and their relevant genotype information are indicated on the left; percentages are indicated on the right; color code below. (c) Absolute live cell numbers at the end of the 72h treatment period. Cell numbers per ml are indicated on the right and correspond to the data plotted in (b).

2.3.2 Genetic validation of the sensitive of GSK-J4 in OCI-AML5

We genetically validated the pharmacological specificity of the H3K27 demethylase inhibitor GSK-J4 using RNAi technology. To this end, we infected OCI-AML5 cells with

lentivirus expressing *shUTX* or *shJMJD3*. Western blot analysis revealed that shRNAs targeting UTX and JMJD3 produced a 50-75% knockdown and an increase in H3K27me2/3 (**Figure 20a and 20b**). To investigate, the impact of knocking down JMJD3 and UTX in OCI-AML5, we tracked sh*JMJD3* tdTomato or *shUTX* GFP marked cells over several passages in a competitive proliferation assay. However, it appeared that there were no changes in percentage of the infected cells that indicated an apoptotic phenotype **(Figure 20c and 20d).** This was not unexpected, since GSK-J4 targets the JMJC domain of UTX and JMJD3. However, OCI-AML5 cells doubly infected with *shUTX* and *shJMJD3* tracked over several passages did not display an alteration in cell proliferation **(Figure 20e)**. We suspected that the lack of an apoptotic phenotype was a result of the remaining protein that was sufficient to sustain cell survival, thereby using tetracycline-inducible Cas9 clones of OCI-AML5, we generated knockouts of JMJD3 or UTX. Infected cells were singularized to generate clonal populations, and the clones were validated for the efficiency of the knockout by western blot which showed that there was a complete deletion of the protein **(Figure 21a and 21b)**. Using JMJD3 knockout OCI-AML5 cells, we then introduced the validated sgUTX lentivirus to generate double knockout OCI-AML5 cells **(Figure 21c)**. However, tracking of single positive or double positive cells did not show any decrease in proliferation that would indicate apoptosis in the infected cells **(Figure 21d).**

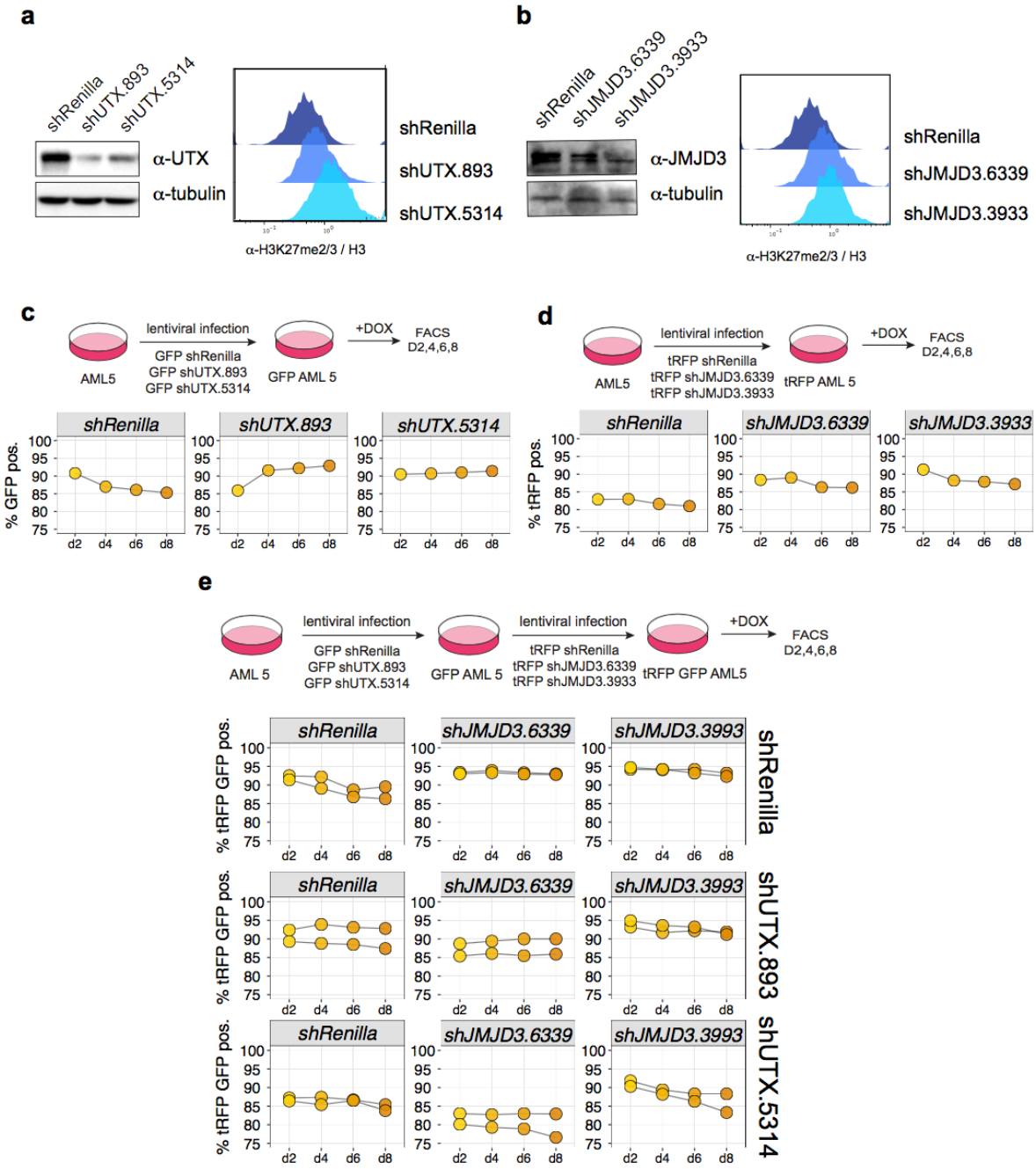

Figure 20. shUTX/JMJD3 validation of pharmacological specificity of GSK-J4 in OCI-AML5. (a-b) Inducible *shUTX IRES GFP* or *shJMJD3 IRES tRFP* were activated upon the addition of doxycycline in media conditions. Following 48 hours doxycycline induction, the knockdowns of UTX/JMJD3 were validated using whole cell lysate. Expression the *shRNA* of H3K27 demethylases led to a corresponding increase in H3K27me3. (c-d) Experimental strategy to assess the proliferative ability of infected OCI-AML5 cells. Transfected OCI-

AML5 cells expressing the shRNA for UTX and JMJD3 were passaged for 8 days to reveal cell proliferation activity (n=1) (e) Experimental strategy to assess the proliferative ability of doubly infected OCI-AML5 cells. OCI-AML5 cells were infected first with shUTX and then *shJMJD3*. Activation of shRNA was induced with doxycycline and passaged for 8 days. n=2

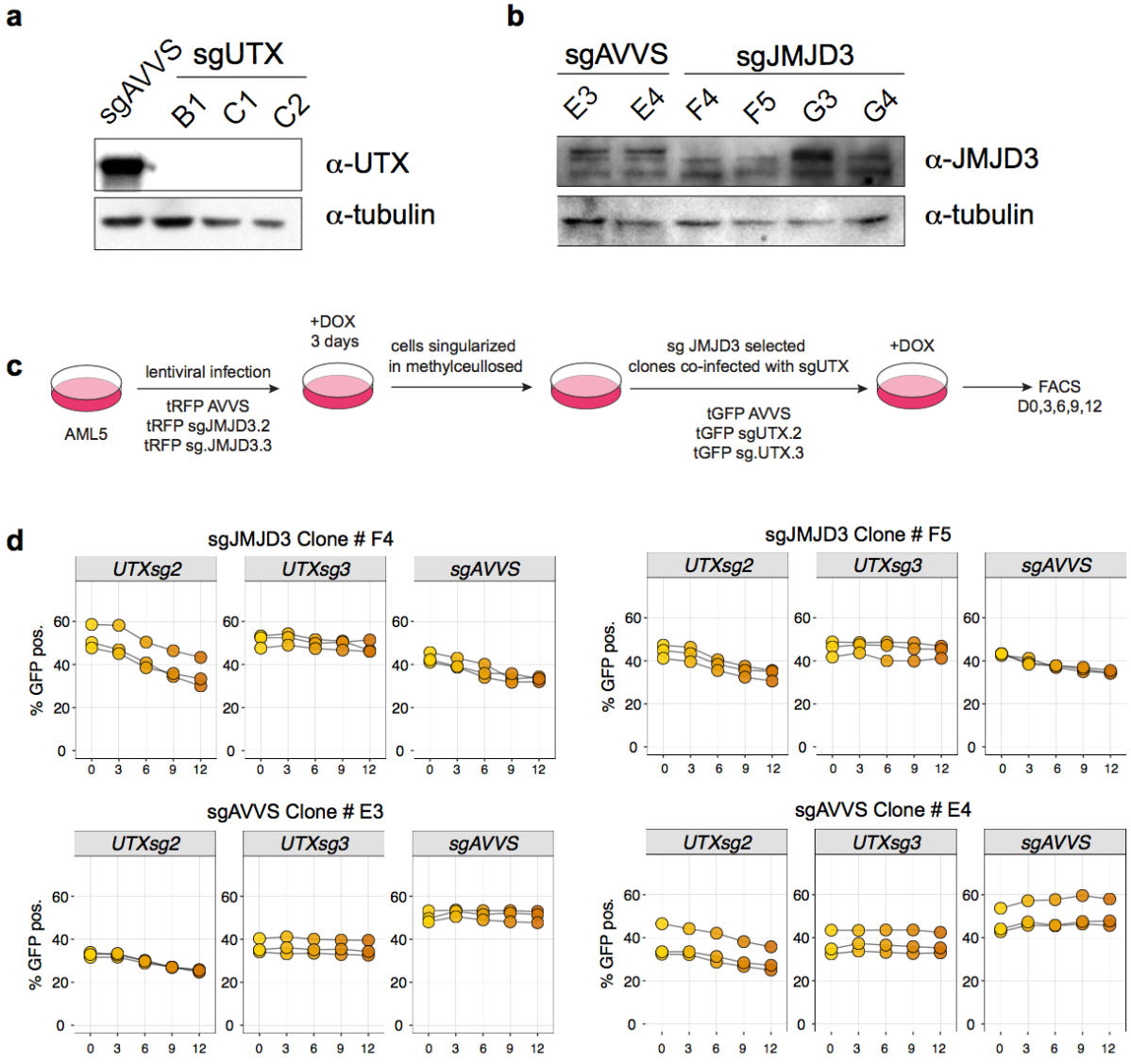

Figure 21. sgUTX/JMJD3 validation of pharmacological specificity of GSK-J4 in OCI-AML5. (a-b) Generation of *sgUTX IRES GFP* or *sgJMJD3 IRES tRFP* OCI-AML5 clones. The inducible Cas 9 was activated upon the addition of doxycycline into media conditions. Following 48 hours doxycycline induction, OCI-AML5 cells were plated into methylcellulose to be singularized and expanded into a clonal population. Knockout of clonal

UTX/JMJD3 populations were validated using whole cell lysates. (c) Experimental strategy to assess the proliferative ability of doubly infected OCI-AML5 cells. OCI-AML5 were infected with lentivirus expressing *sgJMJD3 IRES tRFP, the* inducible Cas9 was activated with doxycycline and then cells were singularized. The singularized clonal population that showed complete JMJD3 knockout were then infected with lentivirus expressing sgUTX. The proliferative ability the double infected cells were monitored through FACS analysis. (d) Summary of the proliferation profiles of JMJD3 and UTX knockout OCI-AML5 cells.

In summary, we had expected UTX/JMJD3 knockouts in OCI-AML5 to phenocopy GSK-J4's apoptotic effect. However, the genetic manipulation of UTX/JMJD3 was unable to validate the specificity of GSK-J4. This highlights the previously implied promiscuity of demethylase inhibitors, more specifically how GSK-J4 could also target the catalytic JMJC domain of other members of the KDM family [67]. Therefore, further genetic validation is needed to understand the mechanisms by which GSK-J4 acts to induce apoptosis in *RUNX1-RUNX1T1* and *RUNX1*^{mut} cells.

CHAPTER 3 – DISCUSSION

Identification of H3K27 mutation in AML

Through our study, we successfully identified and characterized histone H3 lysine 27 missense mutations in the context of acute myeloid leukemia. We show that AML cells with a heterozygous *K27M* mutation in one of twelve canonical H3 genes, *HIST1H3H*, exhibited a reduction in H3K27me2/3 that is reminiscent to that observed in cells lacking the enzymatic activity of EZH2, the major H3K27me2/3 methyltransferase. AML cells with a heterozygous K27I mutation on *HIST1H3F* exhibited a less severe reduction in H3K27me2/3, most likely due to the smaller inhibitory potency of the $H3^{K27I}$ mutation. Hence, the observed biochemical impact of the mutated histone alleles in AML appear to resemble that of the reported histone mutants in glioblastoma cells [47]. In contrast to glioma where H3K27 mutations can occur as frequently as 90% in patient cohorts [48], our data suggests that H3K27 mutations occur at a rare frequency (<1%) in AML (Figure 9d).

Implications of Histone H3 variants in AML

We identified H3 mutations specifically on the H3.1 variant in AML patient samples, but no mutations on either H3.2 or H3.3. However, it should be noted that histone H3.2 and H3.3 are not polyadenylated, and the sequencing of AML patients in the Leucegene database relied on using the polyA tail for sequencing. Therefore, the presence of the H3.2 and H3.3 mutations would have been undetected in our AML patient samples. Interestingly, all three variants of histone H3 have been characterized in glioma patients but are unique in their tumour type, patient age and location. In AML, we would suspect that mutations of other histone variants may also be present but differ in disease characterization (disease latency, infiltration of blast cells, morphology of the disease etc.). Interestingly, while the identified patients had H3.1 mutations that cooperated with RUNX1 alterations, our AML mouse model showed that there was a cooperation between H3.3 and RUNX1 alterations. This also opens up the question of whether the H3.1K27M mutation would behave similar in our AML mouse model and how it would differ from the histone H3.3K27M mutation.

Genetic context of H3K27 mutation in AML

We examined cooperating lesions in $H3^{K27M/I}$ mutated AML patients, and found that they tend to clustered with compromised *RUNX1* gene function. From the characterization and analysis of the $H3^{K27I/M}$ mutations in mouse and human specimens, four key observations were found to support the central notion that $H3^{K27I/M}$ mutations act as secondary lesions that exacerbate leukemia progression following *RUNX1* gene alterations: (i) the predominantly sub-clonal stoichiometry of $H3^{K27I/M}$ mutations in *RUNX1* mutant and *t(8;21)* AML patient samples (ii) promotion of committed myeloid progenitor self-renewal but failure of $H3.3^{K27M}$ expression to cause leukemic transformation *per se*; (iii) promotion of this phenotypic myeloid progenitor self-renewal is also observed when RUNX1 protein expression is diminished; (iv) the significant and selective disease acceleration in an *AML1-ETO9a*-driven *t(8;21)* mouse model. In line with the high frequency of mutations in PRC2-associated genes in AMLs with *RUNX1* gene alterations, our results demonstrate that genetic events causing impaired H3K27me2/3 deposition, either locally or globally are under strong positive selective pressure in *t(8;21)* and *RUNX1* mutant AMLs. Based on this, we propose that the propensity to accumulate secondary lesions that result in reduced H3K27me2/3 is a common hallmark of *RUNX1* altered AMLs.

Characterization and Genetic Validation of GSK-J4 activity

Our results demonstrate that sensitivity to H3K27-demethylases inhibition by GSK-J4 represents a selective and potent vulnerability in AMLs with *RUNX1* gene alterations. While it is tempting to speculate that this sensitivity is a direct consequence of mutated *RUNX1*, we favor the possibility that *RUNX1*-mutant AMLs with reduced PRC2 expression readily become addicted to reduced H3K27me2/3 levels and thus undergo apoptosis upon reversal of this H3K27 hypo-methylation state.

The genetic validation of the presumed targets of GSK-J4 in $RUNX1^{mut}$ OCI-AML5 cells

failed to show hallmarks of decreased cellular proliferation or apoptosis. Through a series of CRISPR-Cas9 and RNAi experiments targeting UTX/JMJD3, it was demonstrated that sensitivity by GSK-J4 in RUNX1^{mut} AML cells observed *in vitro* was most likely due to an off-target effect of GSK-J4. In response to the publication of GSK-J1/J4 as a specific inhibitor of KDM6A/B, *Heinemann et al* raised the concern that GSK-J1/J4 had not been tested for its specificity towards the KDM subfamilies that shared a common JMJC catalytic domain. Their results demonstrate that while GSK-J1 is a highly potent inhibitor of UTX/JMJD3, the molecule has unspecific inhibition towards KDM5B/C (five to ten folds less potent). GSK-J4 was derived from an acid-to-ester group alteration from GSK-J1 to increase cell membrane permeability and this alteration increased GSK-J4's sensitivity towards UTX/JMJD3. However, it was also found to inhibit the catalytic activity of the other tested demethylases including KDM3-5 subfamilies with similar potency. This demonstrated the non-specificity of GSK-J4 and the need for genetic validation when using the inhibitor [67]. There are two possibilities that could explain the contradicting responses between the chemical and genetic approach: (i) the discrepancy between the pharmacological inhibition of the catalytic domain through GSK-J4 vs. the complete genetic deletion of the protein using CRISPR-Cas9/RNAi; (ii) the off targets of GSK-J4 having off targets in addition to H3K27 demethylases (i.e. H3K9 and H3K4 demethylases); (iii) an off target of GSK-J4, and occurs independently of H3K27 demethylases. GSK-J4 has a specific sensitivity towards RUNX1-RUNX1T1/RUNX1^{mut} cell lines that would merit further investigation to delineate the targets of GSK-J4 that causes the anti-tumour response.

To delineate whether the anti-tumour response of GSK-J4 is the result of a gain in lysine 27 methylation and not of another lysine residue, we propose to titrate EZH2 inhibitors (UNC1999 or GSK126) to increase H3K27me2/3 levels in the presence of an apoptosis inducing concentration of GSK-J4. As previously described, the inhibition of UTX/JMJD3 will result in the increase in H3K27me2/3 and apoptosis of RUNX1-RUNX1T1/RUNX1^{mut} cell lines. However, through the addition of EZH1/2 inhibitors H3K27me2/3 will be restored to pre-GSK-J4 levels and should thereby rescue the cells. Overall, this would demonstrate RUNX1-RUNX1T1/RUNX1^{mut} cell survival is dependent on low levels of H3K27me2/3 and that an increase in H3K27me3 through the addition of GSK-J4 is detrimental to the cells. On the other

hand, if the flex of H3K27me3 level in the RUNX1-RUNX1T1/RUNX1^{mut} cell lines does not result in any phenotypically alteration, we will explore the possibility that the phenotype that we observed it is due to the off target effect of GSK-J4.

As previously mentioned, *Heinemann et al* questioned the non-specificity of GSK-J4 as a demethylase inhibitor for lysine 27 and proposed that in addition it nonspecifically inhibited lysine 4 and 9 demethylases [67]. However, given the large number of lysine 4 and 9 demethylases, it is difficult to address the specificity of GSK-J4 through genetically manipulating each of the demethylases either individually and in combination with other demethylases to reproduce the anti-tumour effect observed in RUNX1-RUNX1T1/RUNX1^{mut} cell lines. To address these concerns, we propose to test the sensitivity of GSK-J4 on OCI-AML5 cells that have been infected with the H3.3 lysine-to-methionine mutants. OCI-AML5 cells expressing single histone H3.3 mutants: K4M, K9M, K27M and the double histone H3.3 mutants: K9M/K27M and K4M/K27M would experience a reduction of methylation on the corresponding lysine mark. Assuming the specificity of GSK-J4 towards UTX/JMJD3, OCI-AML5 cells expressing histone H3.3^{K27M} would experience a decrease in H3K27me2/3 and become insensitive to the effect of GSK-J4. However, cells expressing histone H3.3^{K9M} and H3.3^{K4M} would remain sensitive to GSK-J4. If the anti-tumour response that we observed in OCI-AML5 is due to the inhibition of the lysine 9 and 27 demethylase activity, we would expect OCI-AML5 expressing H3.3^{K9M} and H3.3^{K27M} to be sensitive to GSK-J4, and then observe increased sensitivity in OCI-AML5 expressing H3.3$^{K9M/K27M}$ double mutant. This approach using H3.3^{KM} mutants will enable us to delineate which of the demethylases are being targeted by GSK-J4.

Lastly, through genome-wide CRISPR screening technologies using OCI-AML5 cells, we will functionally dissect the genetics of the apoptotic response during H3K27 hypo-methylation from GSK-J4 treatment. Through this unbiased screening approach, we can delineate the essential, suppressor and the enhancer genes that are required to modulate the selectivity to GSK-J4. Assuming the specificity of GSK-J4 towards H3K27 hypermethylation, we would suspect that suppressor genes will include known components of PRC2. If confirmed,

this will strongly suggest that GSK-J4 indeed exerts its activity through re-establishment of H3K27me2/3 in OCI-AML5 cells. This approach would allow the identification of anti-apoptotic genes that are being suppressed due to the gain of H3K27me3 and is driving the apoptotic phenotype that is observed in OCI-AML5. More importantly, it would indefinitely identify the demethylases that are being targeted by GSK-J4, and causing the apoptotic phenotype in OCI-AML5 cells.

The use of AML cell lines to study the clinical relevance of small molecules has been driven by two key components (i) the ease of manipulating cells in culture and (ii) wide availability of cell lines representing the heterogeneity of AML. However, AML cell lines have (i) undergone genetic changes in culture; (ii) no longer retain tumour heterogeneity that was previously present in the primary cancer; (iii) lack several components that are part of the tumour microenvironment. Current opinion suggests that because of these pitfalls it has led to therapies failing early in clinical trials. For further validation of the anti-cancer ability of GSK-J4, we will select human AML specimens based on their genetic make-up (i.e. RUNX1 and PRC2 mutation status) using mutation profiles that have been established through the Leucegene project. These primary AML samples will be maintained in optimized culture conditions including UM729, under these control condition we will test the selectivity of GSK-J4 [68]. In addition, we can employ patient-derived xenografts to efficiently determine the effect of GSK-J4 *in vivo*. These experiments will enable us to consolidate our findings from human AML cell lines in more clinically relevant AML patient samples.

EZH inhibitors in the treatment of RUNX1 altered AML patient

Numerous publications have demonstrated the anti-tumour effect of EZH2 inhibitors in certain genetic contexts [23]. However, our data shows that hypo-H3K27 methylation accelerates the development of RUNX1 altered AML (either RUNX1-RUNX1T1 or $RUNX1^{mut}$). This suggests EZH2 inhibitors that decrease H3K27me2/3 in these patients could potentially be detrimental to their course of treatment.

Interestingly, inhibition of EZH2 has been shown as a potential therapeutic target for $H3^{K27M}$ mutant pediatric gliomas. Although, $H3^{K27M}$ mutations show a global reduction of H3K27me3 levels, many genes still retain H3K27me3 including tumor-suppressor protein p16INK4A. In $H3^{K27M}$ mutated glioma cells, the de-repression of p16INK4A through EZH2 inhibition will abolish the mutated cells [69]. Thereby, suggesting that residual PRC2 activity is required for the maintenance of the tumour. This is in line with the observation that PRC2 mutations have not been documented in glioma. In contrast, we have observed the occurrence of PRC2 and H3K27 mutations in AML, where the mutations appear in similar genetic contexts and function through hypo-H3K27me3. Suggesting, they are interchangeable mutations in the context of $RUNX1^{mut}$ AML. In glioma, the H3K27 mutations are initiating or early mutations. However, our data suggests that H3K27 mutations are secondary mutations in RUNX1 altered AML patients. Given the different genetics of the two cancers, it is difficult to speculate the potential of EZH2 inhibitors in the treatment of RUNX altered AML patients. Therefore, use of EZH2 inhibitors in treating RUNX altered AML is more complex than originally proposed and would merit further investigation. Regardless, it prompts the need to learn about the status of the *RUNX1* gene in patients before administering a treatment. In addition, this highlights the importance of genetic screen and precision medicine in determining a targeted treatment regime for patients with different cytogenetics.

$H3.3^{KM}$ system as a replacement for traditional genetic manipulation of methyltransferase activity

$H3.3^{K27M}$ expression inhibited the enzymatic activity of EZH1/2 in HSPCs and induced a selective expansion of a progenitor population. Using HSPC specific surface markers, the expanded population was characterized as $CD34^{+}CD45RA^{-}CD90^{+}CD133^{-}$. Furthermore, we found that reduced H3K27me3 supported a myeloid progenitor expansion. We have yet to determine the cellular identity of this population because the low frequency of this population has made it difficult to perform cellular assays for its characterization. However, we are in the process of performing RNA-seq experiments using bulk HSPCs expressing the $H3.3^{K27M}$ mutant to further delineate the identity of this population. We suspect that given the pre-leukemic nature

of this population, we will observe an enrichment of genes that are up regulated in RUNX1^{mut} AMLs.

In this study, using the lysine-to-methionine mutants we uncovered the functional impact of loss of histone lysine methylation on normal hematopoiesis, circumventing the traditional approach of targeting the histone methyltransferases. This study has primarily investigated the role of H3K27me3 using H3.3^{K27M} in a primitive population of CD34^{+} cells derived from UCB. Given the dynamic role of H3K27me3 throughout hematopoietic differentiation, we could further investigate the role of H3K27me3 using H3.3^{K27M} expression in different lineages of committed progenitors. Furthermore, this opens the possibility of investigating the role of other histone methylation residues in hematopoiesis using the established histone H3.3^{KM} system.

Uncovering the mechanism behind the genetic synergy of hypo-H3K27me3 and RUNX1 alterations

The underlying mechanism causing the overt genetic collaboration between RUNX1 alterations and hypo-H3K27me3 remains to be uncovered. *Kuvardina et al.* illustrated that RUNX1 repression of erythroid gene expression during megakaryocytic differentiation is dependent on the repression of KLF1 through the simultaneous binding of RUNX1 and EZH2 to the KLF1 promoter [70]. In our context, this introduced the possibility that EZH2 and RUNX1 co-represses a common set of genes. The de-repression of these genes due to the loss of H3K27me3 and RUNX1 binding led to the immunophenotype or acceleration of disease observed in figure 10. We propose to perform ChiP-seq and transcriptome analysis on day 10 expanded UBC cells expressing the H3.3^{K27M} or the shRUNX1. We would expect an overlap of differentially expressed genes that are identified through transcriptome analysis and H3K27me3/RUNX1 binding identified in ChiP-Seq. More importantly, we would expect to identify an overlapping set of deregulated genes in both the conditions, which we suspect would be responsible for the expansion of the described progenitor population. In addition, we hypothesize that this group of deregulated genes are found to be upregulated in RUNX1^{mut} AML. This approach will help elucidate mechanistic underpinnings of this collaboration, and will thus likely provide important functional and molecular insights that may drive

tumorigenesis in RUNX1^{mut} AML.

Concluding remarks

In closing, acute myeloid leukemia is defined by an overwhelming degree of genetic diversity. To improve prospects for AML patients through rationally targeted therapies, it is essential to define molecular parameters that can efficiently identify patients who are most likely to benefit from a given targeted pharmacological intervention. Our results demonstrated that functional impairment of the H3K27 methylation machinery is a specific and powerful collaborating event in AML patients that are characterized by RUNX1 alterations which can be exploited for targeted therapies.

CHAPTER 4 – METHODS

4.1 Primary AML Specimens

The Leucegene project is an initiative approved by the Research Ethics Boards of Université de Montréal and Maisonneuve-Rosemont Hospital. As part of this project, RNA sequencing of 415 primary AML specimens from various cytogenetic groups was performed as previously described 13. All leukemia samples were collected and characterized by the Québec Leukemia Cell Bank (BCLQ).

4.2 Next-generation RNA sequencing and mutation validation.

Sequenced data were mapped to the reference genome hg19 according to RefSeq annotations (UCSC, April 16th 2014). Variants were identified using CASAVA 1.8.2 or km (https://bitbucket.org/iric-soft/km).

3.3 Human cord blood cell collection and processing.

Fresh umbilical cord blood (UCB cells) was collected from consenting donors according to ethically approved procedures at St. Justine, Maisonneuve-Rosemont Hospital (Montréal, QC, Canada) and Charles Le Moyne Hospital (Longueuil, QC, Canada). Human CD34^{+} UCB cells were isolated using the EasySep Human Cord Blood CD34 Positive Selection Kit (STEMCELL Technologies, #18096) through positive selection.

4.4 CD34^{+} cell culture.

Human CD34^{+} cells were cultured in HSC media consisting of StemSpan ACF (STEMCELL Technologies) supplemented with 100 ng/ml human stem cell factor (rhSCF, Shenandoah, #100-04), 100 ng/ml FMS-like trysine kinase 3 ligand (rhFLT3-ligand, Shenandoah, #100-21), 50 ng/ml thrombopoietin (rhTPO, Shenandoah, #100-05), 10 µg/ml human low-density lipoprotein

(LDL, STEMCELL Technologies #02698), 10µg/µl gentamicin (Thermo Fisher Scientific),1x Glutamax (Thermo Fisher Scientific) and UM171 at 35nM (UdeM – IRIC/ STEMCELL Technologies, #72912). For fed-batch experiments, human $CD34^+$ UCB cells were suspended in HSC media with the addition of either vehicle (0.1% DMSO), UNC2400 (1µM, Tocris #4905), UNC1999 (1µM, Tocris #4904) or GSK126 (1µM, Active Biochem #A-1275). $CD34^+$ UCB cells were seeded at 10^5 cells/ml and maintained in 25ml bags (American Fluoroseal Corporation) connected to a syringe loaded pumping system (Harvard Apparatus) and maintained on an orbital shaker at 37°C and in 5% CO_2. Media delivery was set to 1.4µl/min for 10 days.

4.5 Flow-cytometric quantification of H3K27me2/3.

Cells were washed in PBS, pelleted and fixed by drop-wise addition of ice-cold 95% ethanol under vortexing. Cells were immediately placed at 4°C for one hour followed by -20°C for long-term storage. For staining, cells were washed twice and blocked with staining buffer (PBS with 1% BSA and 0.25% Triton). Cells were then stained with mouse monoclonal anti-H3K27me2/3 (Active Motif #39536) and rabbit anti-H3 (Abcam #1791) in staining buffer for 20 min at room temperature. After a wash with staining buffer, cells were incubated with secondary antibodies anti-mouse Alexa-647 (Invitrogen #A-21235) and anti-rabbit Alexa-350 (Invitrogen #A-11046). Cells were washed again and FACS analysis was performed on a BD Biosciences LSR II (IRIC FACS core facility).

Confirmation of H3K27M mutation in patient AML samples. required high and low H3K27me2/3 population to be sorted using the BD FACSARIA III. Preceding cell sort, the isolation of the DNA was performed from a protocol by Zhang el al. The mutated regions were amplified through PCR using the primers indicated in the Appendix.

4.6 Flow cytometric analysis of *ex vivo* cultured UCB cells.

The percentages and absolute numbers of total and gated populations from GFP^+ infected cells were determined by FACS on a BD Biosciences LSRII at 10 days post-infection. Cells were stained with anti-human CD45RA-PE-Cy5 (BioLegend #304110), anti-human CD34-BV421

(BD Biosciences #562577), anti-human CD133-PE (Miltenyi #130-080-801) and anti-human CD90-PE-Cy7 (BioLegend #328124).

For experiments using uninfected $CD34^+$ UCB cells were stained with anti-human CD90-PE-Cy7 (BioLegend #328124), anti-human CD34-FITC (BD Biosciences #555821) and anti-human CD45RA-PE-Cy5 (BioLegend # 304110). Fluorescence was captured on an iQue High Throughput Screener. All subsequent analyses were done on Flowjo v10 (Tree Star).

4.7 Colony forming cell assays.

Frequencies of colony-forming cells were estimated by plating 10^3 sorted GFP^+ UCB cells in 1 ml of 2% methylcellulose-based media in Iscove's Modified Dulbecco's Medium (IMDM) supplemented 10% fetal bovine serum (FBS), 2% bovine serum albumin (BSA), 2 mM L-glutamine, 100 ng/ml SCF, 10 ng/ml IL-3, 10 ng/ml IL-6, 5 ng/ml erythropoietin, 200 µg/ml transferrin and 10^{-4} M 2-mercaptoethanol. After 14 days in culture, plates were visually scored for multi-lineage and granulo/granulo-monocytic colonies.

4.8 Virus Production and UCB Cell Infection.

C-terminally FLAG/HA-tagged H3.3 constructs were obtained from David Allis (Rockefeller U, NY) and cloned into a lentiviral construct containing a full-length human *EF1a* promoter, a downstream *IRES GFP* cassette and a Woodchuck Hepatitis virus posttranscriptional regulatory element (WRE). Lentiviral particles were produced in HEK293T cells. Per 150mm tissue culture dish, 45µg of the lentiviral vector was transiently packaged with 27µg pLP1, 12µg pLP2 and 9µg pVSV-G using Lipofectamine-2000 transfection reagent (Invitrogen). Transfected HEK293T cells were maintained in DMEM with 2% heat-inactivated FBS. Viral supernatant was collected at 48 and 72 hours post-transfection. Virus concentration was achieved by ultra-centrifugation in a Sorvall WX Ultra 100 centrifuge (Thermo Scientific, SureSpin 630 rotor) through a 20% sucrose cushion (32 ml supernatant on top of 5 ml sucrose solution) for 120 min at 4°C and 30,000 rpm. The pelleted virus was reconstituted in PBS (1/100 of the starting volume) and aliquoted and kept at -80°C for long-term storage. Virus titer was typically 10^9 IU/ml as determined on HEK 293T cells. For infection of $CD34^+$ derived UCB cells, non-tissue-culture treated 96-well plates (Sarstedt) were covered with 6.4 µg Retronectin (Takara-

Clontech) in 100µl PBS per well and incubated overnight at 4°C. The coated wells were washed and blocked with PBS containing 2% BSA for 30 min at room temperature. Lentiviral stocks were diluted to a final volume of 100 µl PBS to achieve a multiplicity-of-infection (MOI) of 50, added to the Retronectin-coated wells and centrifuged at 2,000g for 2h at 32°C. The supernatant was then removed and wells were washed once with PBS including 2% BSA. 0.5-1x10^4 UCB cells (24-48h pre-stimulated in HSC media with UM171) cells were placed into lentivirus-preconditioned wells in the presence of 3µg/ml polybrene. 16h post-transduction, cells were washed from the Retronectin with HSC media and placed onto a fresh plate. Transduction efficiency (usually 25-40%) was monitored 48h post infection by GFP-fluorescence on a BD Biosciences Canto II or LSR II.

4.9 Western blot analysis.

Whole-cell extracts from cells treated with EZH1/2 inhibitors or sorted GFP^+ cells were lysed in Laemmli buffer and loaded onto a 14% SDS-PAGE gel at 10^5 cells per lane. Proteins were transferred onto Immobilon-P membrane (Millipore) for 75 minutes at 4°C using an Owl HEP-1 Semi-Dry electro-blotting system (Thermo Scientific). Membranes were blocked with 5% milk protein powder diluted in Tris-buffered saline containing 0.1% Tween-20 (TBST). Blocked membranes were incubated with rabbit anti-H3K27me3 (Millipore #07-449), rabbit anti-H3K27me2 (Millipore #07-452) or anti-H3K9me3 (Active Motif #39161) in TBST plus 5% BSA overnight at 4°C. The membrane were washed three times with TBST, incubated with secondary antibody conjugated to horseradish peroxidase (HRP) in TBST plus 5% milk powder for 1h at room temperature, washed three times in TBST and developed using Immobilon Western Chemiluminescent HRP Substrate (Millipore). Results were captured on an ImageQuant LAS4000 (GE Healthcare Life Sciences). Developed membranes were stripped with ReBlot Strong Antibody Stripping Solution (Millipore) to be re-developed with rabbit anti-H3 (Abcam #1791) as a loading control.

4.10 Transplantation and monitoring of H3.3-infected and EZH1/2 treated UCB cells.

All experimental protocols followed guidelines of the Animal Care Committee of Université de Montréal. $CD34^+$ UCB cells expanded in fed-batch culture or on non-treated multi-well plates (Sarstedt) for 10 days were transplanted by tail vein injection into sub-lethally irradiated (25 cGy, <24 hours before transplantation) 8-12 week old female NSG (NOD.Cg-Prkdc^{scid} Il2rg$^{tm1Wjl/SzJ}$, (005557), Jackson Laboratory) mice. Engraftment of human cells in mouse bone marrow was monitored by flow cytometry at 6, 12 and 24 weeks post-transplantation. At 6 and 12 weeks, mouse bone marrow was collected through femoral aspiration. At 24 weeks, NSG mice were sacrificed and cells from mouse bone marrow were flushed from femurae, tibiae and pelves. Cells were treated with red blood cell lysis buffer, washed with FACS buffer (PBS, 2% FBS, 2mM EDTA) and stained with anti-human CD45-Pacific-Blue (BioLegend #304029), anti-mouse CD45-APC-eFluor780 (eBioscience #47-0453-82), anti-human CD33-PE (BD Biosciences #555450), anti-human CD19-PE-Cy7 (BD Biosciences #557835) and anti-human CD34-APC (BioScience #17-0341). Cells were analyzed on the BD Bioscience Canto II.

4.11 Estimation LT-HSC numbers by limiting dilution analysis.

All limiting dilution analyses were performed using the ELDA software from the Walter and Eliza Hall Institute (WEHI) of Medical Research software (http://bioinf.wehi.edu.au/software/elda/index.html).

4.12 Bone marrow cell transduction and generation of mouse AML models.

Bone marrow cells were extracted from adult C57/B6-congenic Pep3B mice and depleted from lineage-positive cells using biotin-labeled anti-B220, anti-Gr1, anti-Ter119 (Biomedical Research Centre, UCB CELLS Vancouver), and streptavidin-coupled MicroBeads (Miltenyi) on an AutoMACS apparatus (Miltenyi). Lineage-negative cells (<10% of total bone marrow) and transformed mouse cells were cultured in mouse bone marrow medium (IMDM, 10% heat-

inactivated FBS, 100 ng/ml rmSCF (Shenandoah, #200-09), 10 ng/ml rmIL-3 (Shenandoah, #200-01), 10 ng/ml rhIL-6 (Shenandoah, #100-10), 10^{-4} M 2-mercaptoethanol).
Retroviral producer cells (GPE+86) were infected with VSV-G-pseudotyped *MSCV AML1-ETO9a IRES GFP* (addgene #12433) or with *MSCV MLL-AF9 IRES Puro* (sUCB CELLSloned from a construct by Frédéric Barabé, Laval U, Québec) and used for ecotropic transduction of 48h prestimulated mouse bone marrow cells by co-culture in the presence of 6µg/ml polybrene. Infected cells were either FACS-sorted based on GFP expression or puromycin-selected (1.5µg/ml, 3d). Secondary infections with *H3.3 IRES tdTomato* expressing *MSCV* vectors were done by GPE+86 co-culture under the same conditions or by spinoculation (1,000g, 32°C, 2h) with VSV-G pseudotyped Plat-A virus-containing supernatant in the presence of polybrene. The resulting AML cell lines were transplanted into 8-10 weeks old C57/B6 sublethally irradiated (60 cGy) recipient mice. Recipient mice were monitored for enlarged spleens and sacrificed at disease end stage. All procedures were conform with institutional guidelines.

4.13 RNAi and CRISPR-Cas9

Prediction algorithm published from *Fellmann et al* were used to design the shRNAs. The shRNA was expressed from an *MSCV IRES tRFP/GFP* that was under the regulation of a tetracycline on system. The oligo for each shRNA used is indicated in the Appendix.

sgRNA were designed from CRISPR Design, a web tool that was published by the Feng Zhang lab (http://crispr.mit.edu:8079/?).The sgRNA were expressed from an MSCV ires tRFP/GFP, and transfected into an inducible OCI-AML5 Cas9 cell line. The activation of the Cas9 in OCI-AML5 was under the regulation of a tetracycline on system. The clonal selection of knockdown protein colonies were achieved through singularization by plating a limited number of cells in methylcellulose colony forming cell medium. The selection of the clonal deletion than occurred 14 days post-plating and then was further expanded for validation of protein knockout. The sgRNA used for each of the experiments are indicated in the Appendix.

Contributions

Yu Wei Zhang (Y.W.Z); Bernhard Lehnertz (B.L); Isabel Boivin (I.B); Nadine Mayotte (N.M) and Tara MacRae (T.M)

Figure 7: Experiments and analysis performed by Y.W.Z.

Figure 8: Experiments performed by YWZ, and analysis by Y.W.Z and B.L.

Figure 9: Identification of H3K27 mutation by B.L. Bioinformatics analysis by B.L. Validation of mutation by Sanger sequencing done by I.B. Quantification of loss of methylation by Y.W.Z. Sorting of low and low methylation population by Y.W.Z with analysis by B.L.

Figure 10: All experiments and analysis performed by B.L, expect experiments involving quantification of methylation are by Y.W.Z

Figure 11: Experiments performed by Y.W.Z and analysis by B.L

Figure 12: Experiments and analysis performed by B.L.

Figure 13: Experiments performed by YWZ, and analysis by Y.W.Z and B.L

Figure 14: Experiments and analysis performed by Y.W.Z

Figure 15: Experiments performed by Y.W.Z and N.M. Analysis performed by B.L.

Figure 16: Experiments and analysis performed by Y.W.Z and B.L.

Figure 17: Experiments performed by YWZ, and analysis by Y.W.Z and B.L

Figure 18: Experiments performed by YWZ, and analysis by Y.W.Z and B.L

Figure 19: Experiments performed by YWZ, and analysis by B.L

Figure 20: shRNA designed by T.M. Experiments and analysis performed by Y.W.Z

Figure 21: sgRNA designed by B.L. Experiments and analysis performed by Y.W.Z

Bibliographie

1. Luger, K., et al., *Crystal structure of the nucleosome core particle at 2.8[thinsp]A resolution.* Nature, 1997. **389**(6648): p. 251-260.
2. Luger, K., M.L. Dechassa, and D.J. Tremethick, *New insights into nucleosome and chromatin structure: an ordered state or a disordered affair?* Nat Rev Mol Cell Biol, 2012. **13**(7): p. 436-447.
3. Bannister, A.J. and T. Kouzarides, *Regulation of chromatin by histone modifications.* Cell Research, 2011. **21**(3): p. 381-395.
4. Talbert, P.B. and S. Henikoff, *Histone variants [mdash] ancient wrap artists of the epigenome.* Nat Rev Mol Cell Biol, 2010. **11**(4): p. 264-275.
5. Jakovcevski, M. and S. Akbarian, *Epigenetic mechanisms in neurological disease.* Nat Med, 2012. **18**(8): p. 1194-1204.
6. Passarge, E., *Emil Heitz and the concept of heterochromatin: longitudinal chromosome differentiation was recognized fifty years ago.* American Journal of Human Genetics, 1979. **31**(2): p. 106-115.
7. Allis, C.D. and T. Jenuwein, *The molecular hallmarks of epigenetic control.* Nat Rev Genet, 2016. **17**(8): p. 487-500.
8. Saksouk, N., E. Simboeck, and J. Déjardin, *Constitutive heterochromatin formation and transcription in mammals.* Epigenetics & Chromatin, 2015. **8**(1): p. 3.
9. Davie, J.R., *Covalent modifications of histones: expression from chromatin templates.* Current Opinion in Genetics & Development, 1998. **8**(2): p. 173-178.
10. Falkenberg, K.J. and R.W. Johnstone, *Histone deacetylases and their inhibitors in cancer, neurological diseases and immune disorders.* Nat Rev Drug Discov, 2014. **13**(9): p. 673-691.
11. Kato, S., K. Inoue, and M.-Y. Youn, *Emergence of the osteo-epigenome in bone biology.* IBMS BoneKEy, 2010. **7**(9): p. 314-324.
12. *An integrated encyclopedia of DNA elements in the human genome.* Nature, 2012. **489**(7414): p. 57-74.

13. Zhang, Y. and D. Reinberg, *Transcription regulation by histone methylation: interplay between different covalent modifications of the core histone tails.* Genes & Development, 2001. **15**(18): p. 2343-2360.
14. Vakoc, C.R., et al., *Profile of Histone Lysine Methylation across Transcribed Mammalian Chromatin.* Molecular and Cellular Biology, 2006. **26**(24): p. 9185-9195.
15. Dillon, S.C., et al., *The SET-domain protein superfamily: protein lysine methyltransferases.* Genome Biology, 2005. **6**(8): p. 227-227.
16. Nguyen, A.T. and Y. Zhang, *The diverse functions of Dot1 and H3K79 methylation.* Genes & Development, 2011. **25**(13): p. 1345-1358.
17. Schapira, M., *Structural Chemistry of Human SET Domain Protein Methyltransferases.* Current Chemical Genomics, 2011. **5**: p. 85-94.
18. Klose, R.J., E.M. Kallin, and Y. Zhang, *JmjC-domain-containing proteins and histone demethylation.* Nat Rev Genet, 2006. **7**(9): p. 715-727.
19. Rotili, D. and A. Mai, *Targeting Histone Demethylases: A New Avenue for the Fight against Cancer.* Genes & Cancer, 2011. **2**(6): p. 663-679.
20. Cao, R., et al., *Role of Histone H3 Lysine 27 Methylation in Polycomb-Group Silencing.* Science, 2002. **298**(5595): p. 1039.
21. Sauvageau, M. and G. Sauvageau, *Polycomb Group Proteins: Multi-Faceted Regulators of Somatic Stem Cells and Cancer.* Cell stem cell, 2010. **7**(3): p. 299-313.
22. Hong, S., et al., *Identification of JmjC domain-containing UTX and JMJD3 as histone H3 lysine 27 demethylases.* Proceedings of the National Academy of Sciences of the United States of America, 2007. **104**(47): p. 18439-18444.
23. Kim, K.H. and C.W.M. Roberts, *Targeting EZH2 in cancer.* Nat Med, 2016. **22**(2): p. 128-134.
24. Orkin, S.H. and L.I. Zon, *Hematopoiesis: An Evolving Paradigm for Stem Cell Biology.* Cell. **132**(4): p. 631-644.
25. Firth, A.L. and J.X.J. Yuan, *Identification of functional progenitor cells in the pulmonary vasculature.* Pulmonary Circulation, 2012. **2**(1): p. 84-100.
26. Mikkelsen, T.S., et al., *Genome-wide maps of chromatin state in pluripotent and lineage-committed cells.* Nature, 2007. **448**(7153): p. 553-560.

27. Cui, K., et al., *Chromatin Signatures in Multipotent Human Hematopoietic Stem Cells Indicate the Fate of Bivalent Genes during Differentiation.* Cell Stem Cell. **4**(1): p. 80-93.
28. Xie, H., et al., *Polycomb repressive complex 2 regulates hematopoietic stem cell maintenance and differentiation in a developmental stage-specific manner.* Cell stem cell, 2014. **14**(1): p. 68-80.
29. Herrera-Merchan, A., et al., *Ectopic expression of the histone methyltransferase Ezh2 in haematopoietic stem cells causes myeloproliferative disease.* Nature Communications, 2012. **3**: p. 623.
30. Kamminga, L.M., et al., *The Polycomb group gene Ezh2 prevents hematopoietic stem cell exhaustion.* Blood, 2006. **107**(5): p. 2170-2179.
31. Good-Jacobson, K.L., *Regulation of Germinal Center, B-Cell Memory, and Plasma Cell Formation by Histone Modifiers.* Frontiers in Immunology, 2014. **5**: p. 596.
32. Su, I.h., et al., *Ezh2 controls B cell development through histone H3 methylation and Igh rearrangement.* Nat Immunol, 2003. **4**(2): p. 124-131.
33. Mandal, M., et al., *Epigenetic repression of the Igk locus by STAT5-mediated recruitment of the histone methyltransferase Ezh2.* Nat Immunol, 2011. **12**(12): p. 1212-1220.
34. Bonnet, D. and J.E. Dick, *Human acute myeloid leukemia is organized as a hierarchy that originates from a primitive hematopoietic cell.* Nat Med, 1997. **3**(7): p. 730-737.
35. Gilliland, D.G., C.T. Jordan, and C.A. Felix, *The Molecular Basis of Leukemia.* ASH Education Program Book, 2004. **2004**(1): p. 80-97.
36. Østgård, L.S.G., et al., *Reasons for treating secondary AML as de novo AML.* European Journal of Haematology, 2010. **85**(3): p. 217-226.
37. Papaemmanuil, E., et al., *Genomic Classification and Prognosis in Acute Myeloid Leukemia.* New England Journal of Medicine, 2016. **374**(23): p. 2209-2221.
38. *Genomic and Epigenomic Landscapes of Adult De Novo Acute Myeloid Leukemia.* New England Journal of Medicine, 2013. **368**(22): p. 2059-2074.
39. Varambally, S., et al., *The polycomb group protein EZH2 is involved in progression of prostate cancer.* Nature, 2002. **419**(6907): p. 624-629.

40. Bachmann, I.M., et al., *EZH2 Expression Is Associated With High Proliferation Rate and Aggressive Tumor Subgroups in Cutaneous Melanoma and Cancers of the Endometrium, Prostate, and Breast.* Journal of Clinical Oncology, 2006. **24**(2): p. 268-273.
41. Yap, D.B., et al., *Somatic mutations at EZH2 Y641 act dominantly through a mechanism of selectively altered PRC2 catalytic activity, to increase H3K27 trimethylation.* Blood, 2011. **117**(8): p. 2451-2459.
42. McCabe, M.T., et al., *EZH2 inhibition as a therapeutic strategy for lymphoma with EZH2-activating mutations.* Nature, 2012. **492**(7427): p. 108-112.
43. Verma, S.K., et al., *Identification of Potent, Selective, Cell-Active Inhibitors of the Histone Lysine Methyltransferase EZH2.* ACS Medicinal Chemistry Letters, 2012. **3**(12): p. 1091-1096.
44. Konze, K.D., et al., *An Orally Bioavailable Chemical Probe of the Lysine Methyltransferases EZH2 and EZH1.* ACS Chemical Biology, 2013. **8**(6): p. 1324-1334.
45. Ernst, T., et al., *Inactivating mutations of the histone methyltransferase gene EZH2 in myeloid disorders.* Nat Genet, 2010. **42**(8): p. 722-726.
46. Nikoloski, G., et al., *Somatic mutations of the histone methyltransferase gene EZH2 in myelodysplastic syndromes.* Nat Genet, 2010. **42**(8): p. 665-667.
47. Anderton, J.A., et al., *The H3K27me3 demethylase, KDM6B, is induced by Epstein-Barr virus and over-expressed in Hodgkin's Lymphoma.* Oncogene, 2011. **30**(17): p. 2037-2043.
48. Khuong-Quang, D.-A., et al., *K27M mutation in histone H3.3 defines clinically and biologically distinct subgroups of pediatric diffuse intrinsic pontine gliomas.* Acta Neuropathologica, 2012. **124**(3): p. 439-447.
49. Wu, G., et al., *Somatic Histone H3 Alterations in Paediatric Diffuse Intrinsic Pontine Gliomas and Non-Brainstem Glioblastomas.* Nature genetics, 2012. **44**(3): p. 251-253.
50. Lewis, P.W., et al., *Inhibition of PRC2 Activity by a Gain-of-Function H3 Mutation Found in Pediatric Glioblastoma.* Science (New York, N.Y.), 2013. **340**(6134): p. 857-861.

51. Justin, N., et al., *Structural basis of oncogenic histone H3K27M inhibition of human polycomb repressive complex 2.* 2016. **7**: p. 11316.
52. Kruidenier, L., et al., *A selective jumonji H3K27 demethylase inhibitor modulates the proinflammatory macrophage response.* Nature, 2012. **488**(7411): p. 404-408.
53. Hashizume, R., et al., *Pharmacologic inhibition of histone demethylation as a therapy for pediatric brainstem glioma.* Nature medicine, 2014. **20**(12): p. 1394-1396.
54. Ito, Y., S.-C. Bae, and L.S.H. Chuang, *The RUNX family: developmental regulators in cancer.* Nat Rev Cancer, 2015. **15**(2): p. 81-95.
55. Tahirov, T.H., et al., *Structural Analyses of DNA Recognition by the AML1/Runx-1 Runt Domain and Its Allosteric Control by CBF&#x3b2.* Cell. **104**(5): p. 755-767.
56. Kitabayashi, I., et al., *Activation of AML1-mediated transcription by MOZ and inhibition by the MOZ–CBP fusion protein.* The EMBO Journal, 2001. **20**(24): p. 7184-7196.
57. Aikawa, Y., et al., *Roles of HIPK1 and HIPK2 in AML1- and p300-dependent transcription, hematopoiesis and blood vessel formation.* The EMBO Journal, 2006. **25**(17): p. 3955-3965.
58. Mangan, J.K. and N.A. Speck, *RUNX1 mutations in clonal myeloid disorders: from conventional cytogenetics to next generation sequencing, a story 40 years in the making.* Critical reviews in oncogenesis, 2011. **16**(1-2): p. 77-91.
59. Gaidzik, V.I., et al., *RUNX1 mutations in acute myeloid leukemia are associated with distinct clinico-pathologic and genetic features.* Leukemia, 2016. **30**(11): p. 2160-2168.
60. Faber, Z.J., et al., *The genomic landscape of core-binding factor acute myeloid leukemias.* Nat Genet, 2016. **48**(12): p. 1551-1556.
61. Sashida, G., et al., *Ezh2 loss promotes development of myelodysplastic syndrome but attenuates its predisposition to leukaemic transformation.* 2014. **5**: p. 4177.
62. Lavallée, V.-P., et al., *RNA-sequencing analysis of core binding factor AML identifies recurrent ZBTB7A mutations and defines RUNX1-CBFA2T3 fusion signature.* Blood, 2016. **127**(20): p. 2498.
63. Vangala, R.K., et al., *The myeloid master regulator transcription factor PU.1 is inactivated by AML1-ETO in t(8;21) myeloid leukemia.* Blood, 2003. **101**(1): p. 270.

64. Ahn, E.-Y., et al., *Disruption of the NHR4 domain structure in AML1-ETO abrogates SON binding and promotes leukemogenesis.* Proceedings of the National Academy of Sciences, 2008. **105**(44): p. 17103-17108.
65. Ntziachristos, P., et al., *Genetic Inactivation of the PRC2 Complex in T-Cell Acute Lymphoblastic Leukemia.* Nature medicine, 2012. **18**(2): p. 298-301.
66. Fares, I., et al., *Pyrimidoindole derivatives are agonists of human hematopoietic stem cell self-renewal.* Science (New York, N.Y.), 2014. **345**(6203): p. 1509-1512.
67. Heinemann, B., et al., *Inhibition of demethylases by GSK-J1/J4.* Nature, 2014. **514**(7520): p. E1-E2.
68. Pabst, C., et al., *Identification of small molecules that support human leukemia stem cell activity ex vivo.* Nat Meth, 2014. **11**(4): p. 436-442.
69. Mohammad, F., et al., *EZH2 is a potential therapeutic target for H3K27M-mutant pediatric gliomas.* Nat Med, 2017. **23**(4): p. 483-492.
70. Kuvardina, O.N., et al., *RUNX1 represses the erythroid gene expression program during megakaryocytic differentiation.* Blood, 2015. **125**(23): p. 3570-3579.

Appendix

Lentivirus Production and Transduction of CD34+ cord blood cells

Before starting:

 You must read and sign the SOP for working with VSV viruses
All steps following HEK transfection with lentiviral vector have to be done in the amphotropic hood, and cells must be kept in the amphotropic incubator
Pipet any virus media into a bucket containing bleach.
Use only filtered tips when pipetting virus containing solutions
All virus-touching disposables should be rinsed with bleach when done
Spray down work surfaces with peroxigard, and then 70% alcohol after using
For virus production to be good, each of these steps has to be streamlined.
The following protocol can be scaled up or down, as desired, according to the number of HEK cells wanted (approximated by total plate surface area).

This protocol is in 3 parts:

1. Lentivirus production in HEK 293 cells
2. Lentivirus titering on HEK 293 cells
3. Transduction of CD34+ cord blood cells

1. Lentivirus production in HEK 293 cells

Materials and Reagents

(for transfections in 10 cm dish)
Lentiviral vector: need 15ug ea vector / transfection (different backbones are available in the lab: mndu from Keith Humphries lab, pLKO from Sigma TRC mission....).
Packaging vectors: 2nd generation packaging plasmids containing *gag*, *pol*, and *rev* genes (pLp1 and pLp2) and envelope plasmids (choose between VSV.G **or** RDT114 (VSVG will produce higher titers, but RDT env. shows better transduction of human HSC, especially long-term HSCs)
Note that all DNA must be of high quality, with concentrations ≥ 1ug/ul. Large preps should be resuspended in the hood with sterile water.

- pLP1 DNA bank # 2783 9ug/ transfection
- pLP2 DNA bank # 2783 4ug/ transfection
- VSV.G DNA bank # 917 3ug/ transfection
- RDT114 DNA bank # 2811 3ug/ transfection

HEK293 packaging cells (always use when not more than 10 passages)
Lipofectamine 2000 60ul/ transfection

OptiMEM serum free media 20ml/ transfection
DMEM + 10% FBS^{HI} 10ml/ transfection
10cm Falcon dishes 1/ transfection (or other format and scale volumes accordingly)
22 µm filters (yellow) 1/ transfection
10ml syringes 1/ transfection
Filtered pipet tips

PEG-it 5X kit (for virus concentration) 2.5ml /transfection

Cell culture hood and incubator dedicated for work with ampho viruses
Ampho centrifuge in room 1352

Procedure

Day 1: Split packaging cells

Seed HEK293 packaging cells at 5 - 6 x 10^6 cells /10 cm dish in DMEM 10% FBS^{Hi}.
Incubate cells for 24 h or until the following afternoon. After ~24 h, the cells should be ~70% confluent.
Notes: Always transfect freshly split cells, at passage number < 10
HEK293 cells are normally split when 70-90% confluent = about every 3 days at 1:10 – 1:15
Do not let the HEK cells get too confluent as they will form a "aggregates" and will lift very easily

Day 2: Transfect packaging cells

(per 10 cm dish)
In a 14ml tube, add **1mL OptiMEM** plus the appropriate volume of the 4 plasmids:
15ug lentiviral vector
9ug pLp1
4ug pLp2
3ug envelope

➔ If using multiple lenti vectors, make a master mix of the 3 packaging vectors, then aliquot 1ml/ tube and add the lenti vector.

In a separate tube: add **1 ml OptiMEM + 60 µl Lipofectamine**. Mix by flicking the tube (do not mix by pipetting or vortexing).

➔ If doing multiple transfections, make a master mix

Incubate lipofectamine- OptiMEM mixture for **5 min at room temperature**.
Add the diluted lipofectamine to the plasmid mixture and mix by gently flicking the tube.
Incubate the transfection mix for **30 - 45 min at room temperature** (to allow complexes to form).
Meanwhile, Replace media on packaging cells with **8ml OptiMEM** (NO ANTIBIOTICS as it interferes with lentivirus production)

Transfer the 2ml of transfection mix onto the packaging cells dropwise without mixing, taking care to distribute the drops over entire plate. Let the plate sit **5min** before gently swirling and transferring to the **ampho incubator** ⚠
Incubate cells for 18 h (37°C, 5% CO^2), or until the following morning.

Day 3: Remove transfection complexes from cells

In the morning: Change media to remove the transfection reagent and replace with 10ml OptiMEM.

Day 4-5: Collect lentiviral soup at ~48 hours post-transfection

Pipet the virus containing media off packaging cells and transfer it to a 15ml falcon tube.
Spin at **1,250rpm* for 5 min** to pellet any packaging cells that were collected during harvesting. * use the ampho centrifuge with the bucket covers ⚠
Remove the plunger from a 10ml syringe (place the plunger ruber side up in the hood to keep sterile) and attach a yellow 22 µm filter to it, then place the filter-syringe on top of a 50ml falcon tube
Pipet the supernatant into the filter-syringe and use the plunger to push the soup into the falcon tube.
Proceed to Virus concentration, or store the virus as needed

- ➔ Virus may be stored at 4 °C for short periods (up to 4 days), but should be frozen at -80 °C for long-term storage. To reduce the number of freeze/thaw cycles, aliquot large-scale virus preps to smaller storage tubes prior to long-term storage.

Virus concentration (option for infection of hematopoetic cells)

For infection of normal or leukemic hematopoietic cells, lentivirus has to be concentrated (10 to 50 times) with PEG-IT (this protocol) or by ultracentrifugation.
(https://www.systembio.com/downloads/Manual_PEG-it_web_021312.pdf)
To the virus soup, add 5X PEG-IT solution to give 1X final concentration:

Total volume of viral soup ÷ 4 = volume of 5X PEG-IT to add

Put at **4˚C overnight** (in a box in the fridge in room 1352)
Next day:
Centrifuge lentivirus at **1500g, for 30min at 4˚C** (lentivirus particles appear as white or beige pellet – more visible with VSV than with RDT envelope). * use the ampho centrifuge with the bucket covers ⚠

Carefully remove supernatant with a pipet, leaving about 500ul (20X concentration)

Resuspend the virus in this media by pipetting up/down gently with a P-100, avoiding bubble production, as formation of bubbles can ruin virus. Can add more OptiMEM if desired.

Aliquot viruses as needed (keep some for virus titration – *80ul if titering in 6w plates*); 25 to 100ul aliquots, unless large quantities will be needed.

Freeze at **-80°C** for up to 1 year, in a plastic freezer box. During freezing, it is important to use a mammalian cell-freezing box (i.e., which lets temperature drop at ~1°C per minute), for optimal titer preservation. Each freeze / thaw cycle will decrease the viral titer by ½, therefore many people choose to titer the virus after thawing.

2. Lentivirus Titration

Materials and Reagents

(for infections in 6 well plate)

Concentrated virus	80ul undiluted ea virus to titer
HEK293 cells (less than 15 passages)	$2.8x10^6$ cells /virus to titer
DMEM 10% FBS^{hi} +antibiotics	14ml /virus to titer
Polybrene (Stock at 6mg/ml, final conc 6ug/ml)	12ul /virus to titer

6 well Falcon plates (or other plate format – scale volumes accordingly)
Filtered pipet tips

Cell culture hood and incubator dedicated for work with ampho viruses
Ampho centrifuge in room 1352

Procedure

Day 1: Dilution of Virus and infection of HEK293 cells

Titration could be done with other cells (HeLa, Jurkat, KG1a) but might not give same titers, as cells lines are infectable at different MOI

Plate **$4x10^5$ HEK293** cells in **1ml media** / well of 6w plate
You will need 6 wells /virus dilution plus one well for a negative control (can keep only one well for neg ctrl if you have multiple viruses to titer).

Prepare media with **2X polybrene** for your dilutions: Need 7ml + 11.6ul polybrene stock / dilution series (Stock at 6mg/ml, final concentration is 5ug/ml, so 2X= 10ug/ml).

Make **serial dilutions** of virus in media with 2X polybrene as follows, mixing well between each dilution by pipetting up/ down 10 times:

Tube #	1	2	3	4	5	6
2X dilution	1/25	1/50	1/500	1/5,000	1/50,000	1/500,000
Volume diluted virus	80ul stock	600ul	120ul	120ul	120ul	120ul
Volume media	1920ul	600ul	1080ul	1080ul	1080ul	1080ul
Final dil.	1/50	1/100	1/1,000	1/10,000	1/100,000	1/1,000,000

Transfer **1ml** of each dilution to the 6w plate (already containing 1ml media), to make 1X polybrene, and give the appropriate final virus dilutions

➔ Incubate at 37˚C for 48 hours

Day 3: Flow Cytometry and calculation of virus titer

Trypsinize cells:

Wash cells with PBS- if cells are lifting, put PBS wash into FACS tube (later add trypsinized cells to same tube)

Add 500ul pre-warmed trypsin and incubate 2-5min

Inactivate trypsin with 1.5ml media, pipet up and down and transfer to a FACS tube, add additional 3ml media or PBS (=1st wash)

Spin down cells 1,000 rpm 5min, then remove supernatant with a pipet (contains virus!)

⚠ **Cells must be washed twice with 5ml PBS (10X volume) to remove residual virus** * use the ampho centrifuge with the bucket covers

After 2nd wash, leave cells in about 500ul residual PBS

Run flow cytometry to detect GFP (or other flourophore) positive cells

Calculation of virus titer:

Take % infection numbers from dilutions yielding 1-10% infection efficiency.

Formula to have Titer in **IU/mL** =

(#cells at starting time)*(% infection/100) / (dilution)*(volume media + virus (ml))

Example: 7.2% GFP+ obtained with 1/1000 dilution of virus
400,000cells * 0.072 / 0.001dilution * 2ml = $1.44X10^7$ IU/ml

In general, you should have at least $1.0x10^7$ IU/ml with VSVg envelope, or $1x10^6$ IU/ml with RDT envelope

3. Transduction of CD34+ cord blood cells

Materials and Reagents

(For infections in 96 well plate)

CD34+CB cells	2 – 20,000 cells /well
Retronectin (stock at 1ug/ul)	6.4ul /well
PBS	
PBS + 2%BSA (BSA stock at 30%)	200ul /well

StemSpan media with cytokines ** 250ul /well
***See media composition protocol*
+ SCF, FLT3, TPO, LDL, Glutamax, Cipro, gentamicin + UM1
Polybrene (stock at 6mg/ml – for CD34 cells, use at 3ug/ml final= 1/2,000 dil)
OpitMEM up to 100ul / well

Non-treated Sarstedt 96 well tissue culture plates (for suspension cells)
Filtered pipet tips
Multi-channel pipettors
Parafilm

Cell culture hood and incubator dedicated for work with ampho viruses
Centrifuge with plate adaptors at 32˚C

*** protocol for infection in 96w plates, to scale up, infect multiple wells, then pool after infection**

Procedure

Day 1: Coat plates with Retronectin & Thaw cord blood cells

Thaw Stem-span media aliquot and retronectin
Figure out your plate lay-out and determine the total number of wells needed. Remember to include un-transduced control wells, and allow for duplicates or triplicates when appropriate.
Retronectin Coating :
http://www.clontech.com/takara/US/Support/Videos/Gene_Transfer/RetroNectin
Add 10-20ug/cm2 to a non-treated tissue culture -> If expt is done in 96 well plates: surface area of well = 0.32cm2 (0.32*20=**6.4ug/well**) stock at 1ug/ul, so 6.4ul / well

Dilute the retronectin in PBS (6.4ul retronectin /100ul PBS /well)
Ex: If you need 48 wells; dilute 320ul retronectin + 4,680ul PBS = 5ml total
Cover each well to be used with 100ul diluted retronectin
Wrap plate edges with parafilm and leave it overnight at 4˚C
Thawing and prestimulation of cord blood derived CD34+
Determine total number of cells needed for your experiment in order to select appropriate vial to thaw. Want **2- 20,000 cells / well**. Sophie Corneau is in charge of distributing vials of Cord Blood cells, so see her ahead of time with the number of cells you will need (sometimes can share a vial with other lab members).
 Note that these cells come from human patients, and as such should be handled as potentially infections
Thaw vial of cells according to protocol: "***Thawing CD34 Cord blood cells***"
Prestimulate 24 to 48hr culture in SFM + cytokines (+ UM171)

Day 2: Add virus and CD34 cells to plate

Aspirate retronectin and add **100ul / well of PBS+2%BSA** (to block). Keep them at **RT° for 30min**
Aspirate and wash once with PBS
Determine the amount of virus needed to achieve the desired **MOI:**
volume of virus in ul = (# cells / viral titer IU/ml) * MOI IU/cell * 1000 ul/ml
ex. For 10,000 cells at with virus titer of $1.4x10^8$ IU/ml; for MOI of 5 => need 0.3ul virus

Dilute the virus in OptiMEM or PBS (*no serum*) to yield 100ul diluted virus at the desired MOI per well. *If there are multiple wells receiving the same virus, prepare a mastermix for the number of wells needed.*
Load the **100ul of diluted lentivirus** onto the retronectin coated well and seal plate edges with parafilm ⚠
Centrifuge at 2,000g for **2hr at 32˚C** in ampho centrifuge with bucket covers
Remove supernatant by pipetting (multichannel with filter tips), and **wash** the wells once with **100ul PBS + 2%BSA**
Transfer pre-stimulated CD34+CB cells to a falcon tube, pipetting up and down to get a good suspension. **Count** 10ul of a 1:1 dilution with trypan blue
Dilute cell suspension in StemSpan media +cytokines +/-compounds to get appropriate volume (100ul/well) to give desired # of cells / well (ex. 10,000 cells /100ul /well -> so for 48 wells, would dilute 50,000 cells in 5ml total volume) ****Add polybrene to 3ug/ul final concentration****
Note that the volume is not critical, only need to cover the wells.
Plate 100ul of the CD34 cell suspension onto the retronectin-virus coated plate, and put in incubator

Day 2-3: Remove cells from lentiviruses *(replate +/- UM1)*

6-16 hours after infection: wash cells from polybrene and lentivirus residues
Transfer the cells in to a new 96 well plate using a multichannel pipet with filter tips
Wash the initial plate with 50ul IMDM media and add it to the new plate
Spin the new plate for 8min at 800rpm. Remove 2/3 of media (100ul) and add 100ul fresh media WITHOUT polybrene ***(+ or - UM1)***

➔ *At this point wells can be pooled into larger wells:*

- pool wells into tubes and wash twice with 10 volumes IMDM
  - (will remove all virus residue, so you can transfer to a non-ampho incubator, and do not need to wash more before FACS)
- spin down and resuspend and seed in 100ul / # original wells

Return cells to incubator

Day 5: Analyse infection efficiency

Analyse infection efficiency 3-7 days post infection (FACS analysis of CD34, CD45RA and fluorescent protein expressed by your lentivirus GFP, YFP, Ametrine…)

⚠ Cells must be fixed in 1% PFA or washed twice with 10X PBS before going to FACS to remove residual virus

This can be done by transferring cells to mini-FACS tubes after Ab staining, and washing / spinning in the tube boxes sealed with parafilm. Remove wash with multichannel pipet in multiple steps (250ul at a time)

You also can keep some cells for further analysis: cell expansion, CFC, transplantation…

Media Composition for infection and maintenance of CD34+ CB

	Stock Location	stock concentration	final concentration	dilution	per mL of media	for 40 mL	
Already mixed in frozen media aliquots: (in chest freezer)							
SCF	-20◦	100 µg/mL	100 ng/mL	1/1000	1µL	40µL	
FLT3	-20◦	100 µg/mL	100 ng/mL	1/1000	1µL	40µL	
TPO	-20◦	100 µg/mL	50 ng/mL	1/2000	0.5µL	20µL	
To be added after thawing:							
LDL	4◦ TC	5 mg/mL	10 µg/mL	1/500	2µL	80µL	
glutamax	RT shelf	100X	1X	1/100	10µL	400µL	
Pen-Strep	4◦ TC	10mg/ml	10ug/ml	1/2000	0.5µL	20µL	
Gentamicin	RT shelf	50mg/mL	50ug/ml	1/2000	0.5µL	20µL	
**** UM1**	-20◦fedbatch	35uM	35nM 1/1000	1/1000	35nM	40µL	1µL

** UM1 is added during infection to achieve maximum infection efficiency -> once cells are removed from viruses on day 2-3, can culture them with or without UM1 depending on the experiment. If comparing +/-UM1, must add 1/1000 volume of DMSO to –UM1 condition.

RNAi and CRISPR-Cas9

shRNA

	Oligo
KDM6A.893	TGCTGTTGACAGTGAGCGCTGGGCTTATGTTCAAAGTGAATAGTGAAGCCACAGATGTATTCACTTTGAACATAAGCCCAATGCCTACTGCCTCGGA
KDM6A.5314	TGCTGTTGACAGTGAGCGCAAGGAGTTCTGTAATTTCAAATAGTGAAGCCACAGATGTATTTGAAATTACAGAACTCCTTATGCCTACTGCCTCGGA
KDM6B.3933	TGCTGTTGACAGTGAGCGCAAGGTTTTAAAGAAAGAACTATAGTGAAGCCACAGATGTATAGTTCTTTCTTTAAAACCTTTTGCCTACTGCCTCGGA
KDM6B.3933	TGCTGTTGACAGTGAGCGACAGCATCTATCTGGAGAGCAATAGTGAAGCCACAGATGTATTGCTCTCCAGATAGATGCTGGTGCCTACTGCCTCGGA
Runx1.4620	TGCTGTTGACAGTGAGCGCTCGCTAAATATTGTAGAAGAATAGTGAAGCCACAGATGTATTCTTCTACAATATTTAGCGAATGCCTACTGCCTCGGA
Runx1.2307	TGCTGTTGACAGTGAGCGCAAGATCCAAATAGAAGAGTTATAGTGAAGCCACAGATGTATAACTCTTCTATTTGGATCTTTTGCCTACTGCCTCGGA

sgRNA

	shRNA (sense strand)
KDM6A_e23	CACCGTTTGTGCGTGTCGTATCAGC
KDM6A_e23	CACCGGATACGACACGCACAAAAGC
KDM6A_e23	CACCGAACTGTGTTCATGCCCAATA
KDM6B_e17	CACCGCGTGGATGTTACCCGCATGA
KDM6B_e17	CACCGCTTCATGCGGGTAACATCCA
KDM6B_e18	CACCGGCGAACCACTCGCAGTCGCC